

AD-A260 794



WL-TR-92-4062

**CHARACTERIZATION OF AEROSPACE GRADE RESINS
AND COMPOSITES THROUGH PRESSURIZED
VOLUMETRIC DILATOMETRY**



**J.D. Russell
D.B. Curliss**

**Structural Materials Branch (WL/MLBC)
Nonmetallic Materials Division**

July 1992



Final Report for Period December 1990 - July 1992

Approved for public release; distribution is unlimited.

93-02271



**MATERIALS DIRECTORATE
WRIGHT LABORATORY
AIR FORCE MATERIEL COMMAND
WRIGHT-PATTERSON AIR FORCE BASE OHIO 45433-6533**


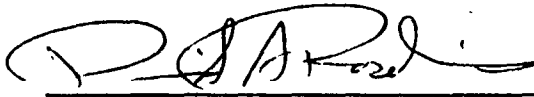

033

NOTICE

When Government drawings, specifications, or other data are used for any purpose other than in connection with a definitely Government-related procurement, the United States Government incurs no responsibility or any obligation whatsoever. The fact that the government may have formulated or in any way supplied the said drawings, specifications, or other data, is not to be regarded by implication, or otherwise in any manner construed, as licensing the holder, or any other person or corporation; or as conveying any rights or permission to manufacture, use, or sell any patented invention that may in any way be related thereto.

This report is releasable to the National Technical Information Service (NTIS). At NTIS, it will be available to the general public, including foreign nations.

This technical report has been reviewed and is approved for publication.


JOHN D. RUSSELL, Chemical Engineer
Composites Section
Structural Materials Branch
DAVID A. ROSELIUS, Chief
Structural Materials Branch
Nonmetallic Materials Division
CHARLES E. BROWNING, Chief
Nonmetallic Materials Division
Materials Directorate

If your address has changed, if you wish to be removed from our mailing list, or if the addressee is no longer employed by your organization please notify WL/MLBC, WPAFB, OH 45433-6533 to help us maintain a current mailing list.

Copies of this report should not be returned unless return is required by security considerations, contractual obligations, or notice on a specific document.

REPORT DOCUMENTATION PAGE			Form Approved OMB No. 0704-0188	
Public reporting burden for this collection of information is estimated to average 1 hour per response, including the time for reviewing instructions, searching existing data sources, gathering and maintaining the data needed, and completing and reviewing the collection of information. Send comments regarding this burden estimate or any other aspect of this collection of information, including suggestions for reducing this burden, to Washington Headquarters Services, Directorate for Information Operations and Reports, 1215 Jefferson Davis Highway, Suite 1204, Arlington, VA 22202-4302, and to the Office of Management and Budget, Paperwork Reduction Project (0704-0188), Washington, DC 20503.				
1. AGENCY USE ONLY (Leave blank)	2. REPORT DATE July 1992	3. REPORT TYPE AND DATES COVERED Final Report/December 1990 - July 1992		
4. TITLE AND SUBTITLE Characterization of Aerospace Grade Resins and Composites Through Pressurized Volumetric Dilatometry		5. FUNDING NUMBERS In-House PE: 62102F Project: 2419 Task: 0310 WU: 45		
6. AUTHOR(S) John D. Russell and David B. Curliss		8. PERFORMING ORGANIZATION REPORT NUMBER WL-TR-92-4062		
7. PERFORMING ORGANIZATION NAME(S) AND ADDRESS(ES) Structural Materials Branch (WL/MLBC) Nonmetallic Materials Division Wright Laboratory Wright-Patterson AFB OH 45433-6533		10. SPONSORING / MONITORING AGENCY REPORT NUMBER		
9. SPONSORING / MONITORING AGENCY NAME(S) AND ADDRESS(ES)		11. SUPPLEMENTARY NOTES		
12a. DISTRIBUTION / AVAILABILITY STATEMENT Approved for public release; distribution is unlimited.		12b. DISTRIBUTION CODE		
13. ABSTRACT (Maximum 200 words) The technique of Pressurized Volumetric Dilatometry has been used to characterize the specific volume changes over pressure and temperature of several state-of-the-art aerospace thermoplastic and thermoset resins and composites and several pitch precursors for carbon-carbon composites. The materials studied were poly(etheretherketone) PEEK; HTA; HTX; PBO/PEEK; 3501-6 epoxy; AS4/3501-6 prepreg; IM7/8551-7A prepreg; IM7/5250-2 prepreg; Ashland Oil pitches A-240, A-60, A-70, and A-80; Reilly Coal Tar; and Mitsubishi's AR Synthetic Mesophase Pitch. Accurate and reproducible Pressure-Volume-Temperature (PVT) data have been yielded by this technique. Important processing information such as T _g (P), CTE(T,P), T _m (P), T _c (P), cure shrinkage, and other phase changes which give rise to volume changes can be extracted from the PVT data.				
14. SUBJECT TERMS Pressurized Volumetric Dilatometry, Cure Shrinkage, Thermoplastics, Thermosets, Pitch			15. NUMBER OF PAGES 95	
17. SECURITY CLASSIFICATION OF REPORT UNCLASSIFIED			16. PRICE CODE	
18. SECURITY CLASSIFICATION OF THIS PAGE UNCLASSIFIED		19. SECURITY CLASSIFICATION OF ABSTRACT UNCLASSIFIED		20. LIMITATION OF ABSTRACT UL

ACKNOWLEDGEMENTS

We wish to thank Frances Abrams from WL/MLBC; Byeongsook Seo from the Air Force Academy; Mick Arnett from Iowa State University; Debbie Gill from the University of Dayton; Dave Anderson, Ron Cornwell, Ken Lindsay, and Bill Price from the University of Dayton Research Institute; and Jim Thomas from McDonnell Douglas for their contributions to this effort.

DTIC QUALITY INSPECTED 3

Accession For	
NTIS GRA&I	<input checked="checked" type="checkbox"/>
DTIC TAB	<input type="checkbox"/>
Unannounced	<input type="checkbox"/>
Justification	
By	
Distribution/	
Availability Codes	
Dist	Avail and/or Special
A-1	

TABLE OF CONTENTS

ABSTRACT	i
ACKNOWLEDGEMENTS	iii
LIST OF ILLUSTRATIONS	ix
LIST OF TABLES	xii
CHAPTER	
1. INTRODUCTION	1
2. BACKGROUND	3
a. PVT Properties of Polymers	3
b. Effect of Time	3
c. Effect of Crystallinity	5
d. Effect of Pressure	5
e. Effect of Cure Shrinkage	9
f. Measuring PVT Properties of Polymers	12
g. Microdielectrometry	12
3. EXPERIMENTAL METHODS	13
a. Materials	13
(1) Thermoplastic Polymers	13
(2) Pitch Precursor for Carbon-Carbon Composites	13
(3) Thermoset Polymers	14
b. RDS-II Dynamic Spectrometer	14
c. Differential Scanning Calorimetry	16
d. Autoclave Cure Monitoring	16

e. PVT Apparatus	16
(1) Equipment Description	16
(2) Isothermal Operation	19
(3) Isobaric Operation	20
4. THERMOPLASTIC RESULTS	21
a. HTA	21
(1) Isothermal Run	21
(2) Isothermal Pressure Dependence of HTA T_g	24
(3) Thermal Expansion of HTA	24
(4) HTA Isobaric Runs	28
(a) Isobaric Pressure Dependence of HTA T_g	28
(b) Densification of HTA During Pressurized Cooling	28
b. PEEK	31
(1) PEEK Isothermal Run	31
(2) Isothermal Pressure Dependence of PEEK T_g	34
(3) Thermal Expansion of PEEK	34
(4) PEEK Isobaric Runs	34
(a) Isobaric Pressure Dependence of PEEK T_g	34
(b) Densification of PEEK During Pressurized Cooling	38
(c) Melting and Crystallization of PEEK	38
c. HTX	39
(1) Isothermal Run	39
(2) Isothermal Pressure Dependence of HTX T_g	42
(3) Thermal Expansion of HTX	42
d. PBO/PEEK	45
(1) Isothermal Run	45
(2) Isothermal Pressure Dependence of PBO/PEEK T_g	45

(3) Thermal Expansion of PBO/PEEK	48
e. Conclusions	48
5. PITCH RESULTS	52
a. A-240	52
b. A-60	52
c. A-70	55
d. A-80	55
e. Reilly Coal Tar	55
f. Mitsubishi AR Synthetic Mesophase	55
g. Conclusions	60
6. THERMOSET RESULTS	61
a. 3501-6	61
(1) Dilatometry	61
(2) Rheology	66
(3) Microdielectrometry	66
b. 8551-7A	68
(1) Dilatometry	68
(2) Rheology	70
(3) Microdielectrometry	70
c. 5250-4	70
(1) Dilatometry	70
(2) Rheology	73
(3) Microdielectrometry	73
d. Conclusions	73
7. CONCLUSIONS	76
a. Future Work	76
(1) Morphology of Densified PEEK	76

(2) Dilatometric Study of APC-2 Under Different Processing Conditions	76
(3) Dilatometric Study of Condensation Curing Resins	77
REFERENCES	78

LIST OF ILLUSTRATIONS

1. Polymer specific volume as a function of temperature.	4
2. Polymer contraction over time after cooling from high above T_g to the indicated temperature.	6
3. Specific volume of polysulfone (amorphous polymer) and poly(ethylene terephthalate) (semicrystalline polymer) as a function of temperature at atmospheric pressure.	7
4. Effect of pressure on the specific volume of polysulfone as a function of temperature during isothermal pressurization at several temperatures.	8
5. Effect of pressure on the specific volume of poly(vinyl acetate) as a function of temperature during isobaric cooling from the melt.	10
6. Volume change during cure of a conventional polyester resin.	11
7. Schematic of the PVT apparatus.	17
8. PVT apparatus with pumps, high-pressure gauge, and associated computer equipment.	18
9. Unassembled piezometer cell.	18
10. PVT properties of HTA.	22
11. DMA scan of HTA	23
12. Isothermal and isobaric dependence of the HTA T_g on pressure.	25
13. PVT properties of HTA at 80 MPa from isothermal data.	26
14. PVT properties of HTA at 90 MPa from isothermal data.	27
15. CTE dependence on pressure of HTA	29
16. Isobaric runs of HTA at 10, 50, and 150 MPa.	29

17. Isothermal PVT properties of PEEK.	32
18. DMA scan of PEEK.	33
19. Dependence of the PEEK T_g on pressure from isothermal data.	35
20. Pressure dependence of CTE of PEEK.	35
21. Isobaric runs of PEEK at 10, 50, and 100 MPa.	37
22. Isobaric pressure dependence of T_m and T_c for PEEK.	40
23. Isothermal PVT properties of HTX.	41
24. Pressure dependence of the HTX T_g on isothermal data.	43
25. Pressure dependence of the HTX CTE.	43
26. PVT properties of PBO/PEEK.	46
27. Pressure dependence of the PBO/PEEK T_g on isothermal data.	47
28. Pressure dependence of the PBO/PEEK CTE.	50
29. Ten MPa isobaric scan of Ashland's A-240 Pitch.	53
30. DSC scan of Ashland's A-240 Pitch.	53
31. Ten MPa isobaric scan of Ashland's A-60 Pitch.	54
32. DSC scan of Ashland's A-60 Pitch.	54
33. Ten MPa isobaric scan of Ashland's A-70 Pitch.	56
34. DSC scan of Ashland's A-70 Pitch.	56
35. Ten MPa isobaric scan of Ashland's A-80 Pitch.	57
36. DSC scan of Ashland's A-80 Pitch.	57
37. Ten MPa isobaric scan of Reilly Coal Tar Pitch.	58
38. DSC scan of Reilly Coal Tar Pitch.	58
39. Ten MPa isobaric scan of Mitsubishi's AR Synthetic Mesophase Pitch.	59
40. DSC scan of Mitsubishi's AR Synthetic Mesophase Pitch.	59
41. Effect of cure cycle on the volume changes in 3501-6 resin.	62
42. Effect of cure cycle on the volume changes in undebulked AS4/3501-6 prepreg.	62

43. Effect of cure cycle on the volume changes in debulked AS4/3501-6 prepreg.	63
44. PMG of the undebulked AS4/33501-6 sample cured in the PVT apparatus.	65
45. DMA scan of AS4/3501-6 prepreg.	67
46. Dielectric loss factor response of AS4/3501-6 prepreg during cure.	67
47. Effect of cure cycle on the volume changes in IM7/8551-7A prepreg.	69
48. DMA scan of IM7/8551-7A prepreg.	67
49. Dielectric loss factor response of IM7/8551-7A prepreg during cure.	67
50. Effect of cure cycle on the volume changes in IM7/5250-4 prepreg.	69
51. DSC scan of IM7/5250-4 prepreg.	72
52. DMA scan of IM7/5250-4 prepreg.	74

LIST OF TABLES

1. Cure cycle for 3501-6, 8551-7A, and 5250-4.	15
2. Coefficients of the volume-temperature equations for the glassy region of HTA.	30
3. Coefficients of the volume-temperature equations for the glassy region of PEEK.	36
4. Coefficients of the volume-temperature equations for the glassy region of HTX.	44
5. Coefficients of the volume-temperature equations for the glassy region of PBO/PEEK.	49

CHAPTER 1

INTRODUCTION

There are many structural and nonstructural applications in which polymers and their composites are being used by the Air Force, and new polymers are continually developed to meet advanced applications. Both polymers and their high performance fiber reinforced composites are attractive as replacements for metals because of their high strength-to-weight and stiffness-to-weight ratios. Since polymers are being used as structural materials, the mechanical behavior and lower cost potential of the materials need to be known. The mechanical behavior of polymers is sensitive to processing history variables such as cooling rate and pressure.

Advanced processing techniques for polymers and polymer matrix composites will require detailed information on the thermodynamic state of the system in order to optimize the properties of components fabricated from these materials. Some significant factors in the component's mechanical behavior and properties are cure shrinkage, coefficient of thermal expansion (CTE) mismatch between the fiber and the matrix, crystallization induced volume changes, and pressure induced volume changes. It is believed that the development of intelligent process control strategies that incorporate these phenomenological changes will result in the production of advanced polymer and composite components with optimum quality and cost. The approach to such a phenomenological based control system requires that we understand a great deal of information such as how the volume of a material changes during processing in response to temperature and pressure, and what its corresponding mechanical properties are during these state changes.

The objective of this study was to characterize the pressure-volume-temperature (PVT) behavior of several materials. The three classes of materials studied were thermoplastic polymers, pitch based precursors for carbon-carbon composites, and thermoset polymers and their composites. A volumetric dilatometer was used to measure the specific volume of the materials as a function of temperature and pressure. When this type of information is combined with the temperature and pressure dependent mechanical properties of the polymer, it can be used to optimize processing of fiber reinforced composites.

CHAPTER 2

BACKGROUND

a. PVT Properties of Polymers

The glass transition temperature (T_g) of a polymer is the point of discontinuity in the coefficient of thermal expansion (α). As the polymer cools from the liquid state through T_g , free volume collapses due to configurational adjustments and eventually becomes small enough that more adjustments are very slow¹. Below T_g , the polymer exhibits glassy behavior, while above T_g , the polymer exhibits rubbery behavior. Many experimental methods are used to measure the T_g of a polymer, such as Differential Scanning Calorimetry (DSC), Dynamic Mechanical Analysis (DMA), Thermomechanical Analysis (TMA), and Volumetric Dilatometry. In Volumetric Dilatometry, T_g can be illustrated by plotting the specific volume, V , of the polymer against temperature, T , (Figure 1)². The point of discontinuity in the slope of this plot is T_g .

b. Effect of Time

As discussed earlier, the small free volume of the glassy state inhibits polymer chain mobility. Struik³ indicates that when a polymer is cooled below T_g , it is not in an equilibrium state, and the initial free volume is greater than the equilibrium free volume. Since mobility is not zero, the amount of free volume will reduce over time. This contraction is accompanied by decreasing mobility. This phenomenon is known as physical aging. Kovacs², in his experiments, displayed the change in polymer specific volume over time. Polymer samples were equilibrated above T_g and then were cooled to a

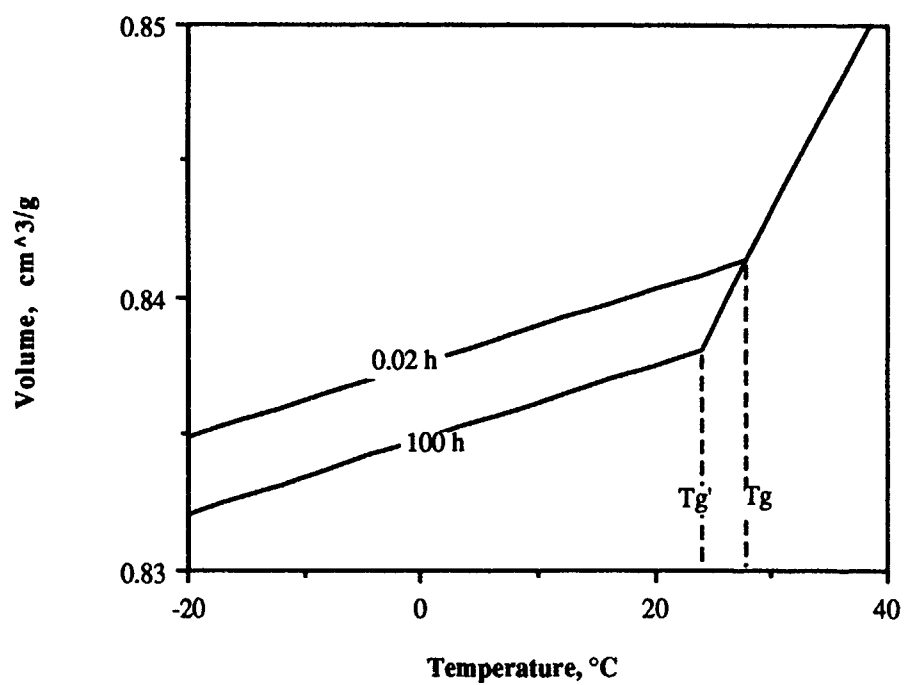


Figure 1. Polymer specific volume as a function of temperature. Volume measured at cooling times of 0.02 and 100 hours².

temperature, T_1 , which was below but near T_g . Over time, the polymer slowly contracts to an equilibrium volume, $V(\infty)$, if T_1 is not far from T_g (Figure 2)². $V(\infty)$ is the remaining specific volume in a polymer after relaxations are complete. The greater the temperature, the shorter the time required for the polymer to reach $V(\infty)$. The effect of annealing time is also discussed by Kovacs². The volumes at cooling times of 0.02 hr and 100 hr are plotted in Figure 1. Longer annealing times result in smaller specific volumes and lower T_g 's than the volumes and T_g 's at shorter annealing times. At longer annealing times, the polymer contracts toward $V(\infty)$ ². Studies indicate that the effect of cooling rates on specific volume and T_g is similar to the effect of annealing time on specific volume and T_g ³⁻⁶. Fast cooling rates correspond to short annealing times, and slow cooling rates correspond to long annealing times.

c. Effect of Crystallinity

The effect of crystallinity on specific volume is displayed in Figure 3⁷. The specific volumes of poly(ethylene terephthalate) (PET), a semicrystalline polymer, and polysulfone, an amorphous polymer, at atmospheric pressure are plotted against temperature. The density change with temperature in the amorphous polymer is on the order of tenths of a percent while, in the semicrystalline polymer, it is on the order of several percent. Furthermore, PET supercools below the melting point temperature (T_m) to a crystallization temperature (T_c). This phenomenon is a characteristic of all semicrystalline polymers. The amount of supercooling is affected by nucleating sites and cooling rates. The degree of crystallinity decreases with increasing cooling rate. For example, at cooling rates above 2000°C/min, poly(etheretherketone) (PEEK), normally a semicrystalline polymer, vitrifies into an amorphous glassy polymer because the polymer molecules are not given sufficient time to align in a crystalline structure⁸.

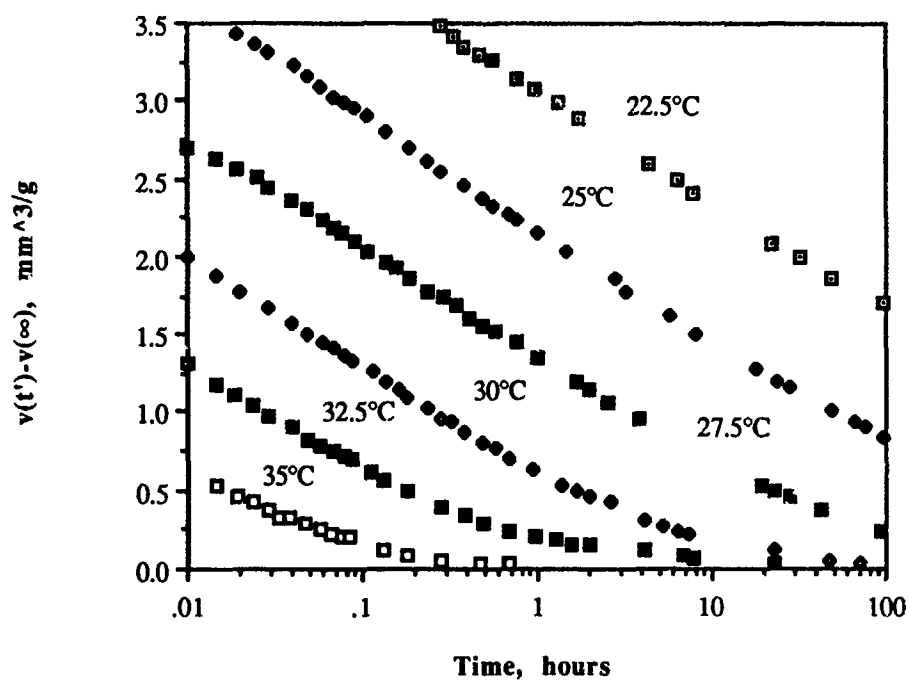


Figure 2. Polymer contraction over time after cooling from high above T_g to the indicated temperature. Data from Kovacs².

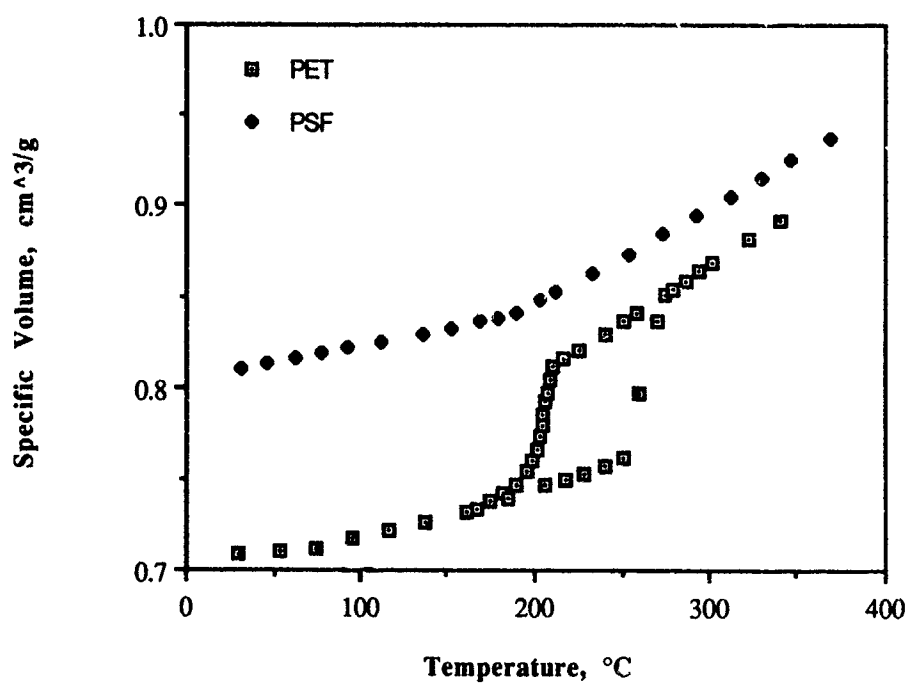


Figure 3. Specific volume of polysulfone (amorphous polymer) and poly(ethylene terephthalate) (semicrystalline polymer) as a function of temperature at atmospheric pressure. Data from Nairn and Zoller⁷.

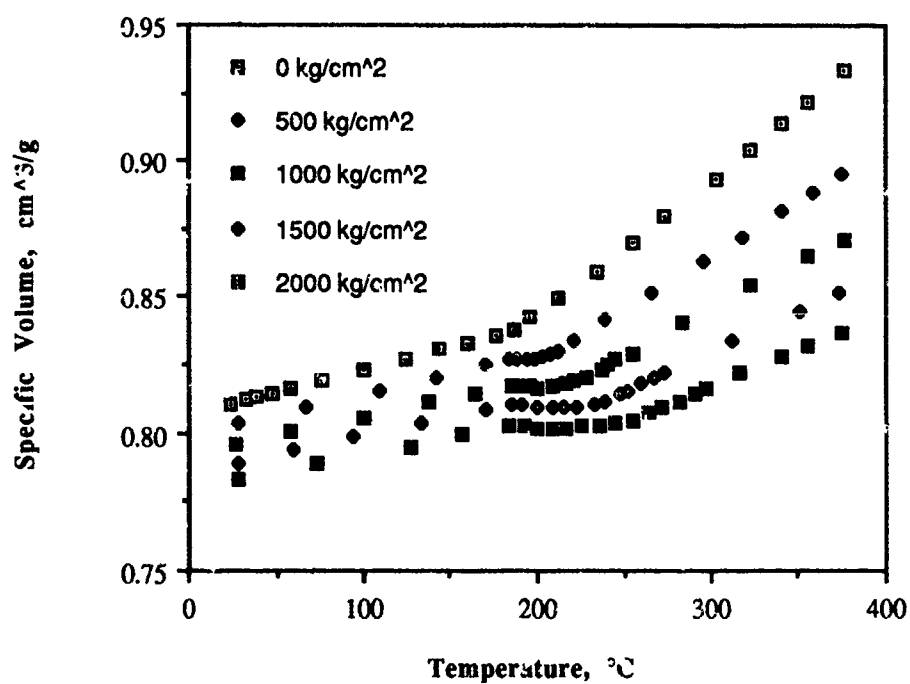


Figure 4. Effect of pressure on the specific volume of polysulfone as a function of temperature during isothermal pressurization at several temperatures. Data from Zoller⁹.

d. Effect of Pressure

The effect of pressure on the specific volume of polysulfone is displayed in Figure 4⁹. As pressure increases, T_g increases and specific volume decreases. The volume changes were measured along isotherms starting at 30°C. The volumes at atmospheric pressure were extrapolated from the data at 100 to 2000 kg/cm². The curved portion of the data between line B and line C results from different types of glasses at each isotherm than the glass formed at low pressure. When a polymer is cooled from the melt state at very high pressures, densified glasses are formed. These glasses have greater densities than the original glass formed at lower pressures⁹⁻¹⁷. These are nonequilibrium states and equations of state based on thermodynamic equilibrium are difficult to apply to this region of data⁹. However, if polymer samples are cooled from the melt along isobars, curves like that of poly(vinyl acetate) in Figure 5 result¹². Each isobar is a different type of glass that has been cooled from the melt state. Literature on PVT data is available on polysulfone⁹, poly(vinyl acetate)¹², PEEK¹⁸, poly(2,6-dimethyl-1,4-phenylene ether)/polystyrene blends¹², polytetrafluoroethylene^{16,17}, low-density polyethylene¹⁸, poly(ethylene terephthalate)²², polystyrene¹⁰, phenoxy¹⁶, bisphenol-a polycarbonate¹⁶, and polyarylate¹⁶. In addition, Curro²³ lists several references on PVT data of polymers.

e. Effect of Cure Shrinkage

Combining the high cure shrinkage of aerospace resins with the low coefficient of thermal expansion (CTE) of high strength fibers results in residual stress. This residual stress is then relieved by several mechanisms such as surface waviness, warping, delamination, and microcracking. The volume change during the cure of a conventional polyester resin is displayed in Figure 6²⁴. Cure shrinkage of the thermosets can be divided into polymerization and thermal shrinkage. Thermal expansion is seen at point 1 as the polymer is heated. Polymerization shrinkage (point 2) occurs during crosslinking and depends on the chemical composition and the polymerization reaction (i.e., addition vs.

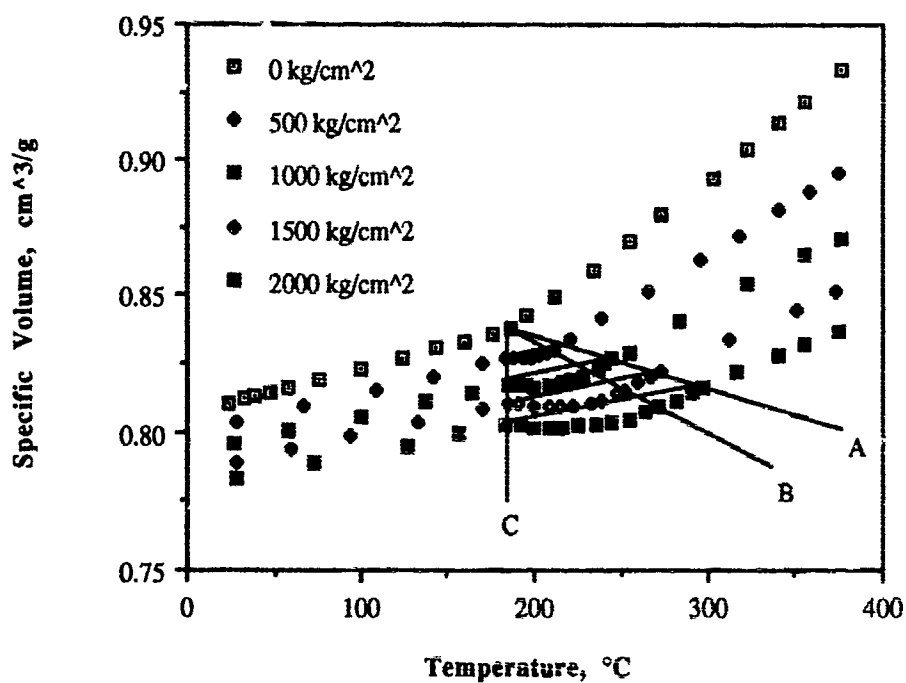


Figure 5. Effect of pressure on the specific volume of poly(vinyl acetate) as a function of temperature during isobaric cooling from the melt. Data from McKinney and Goldstein¹².

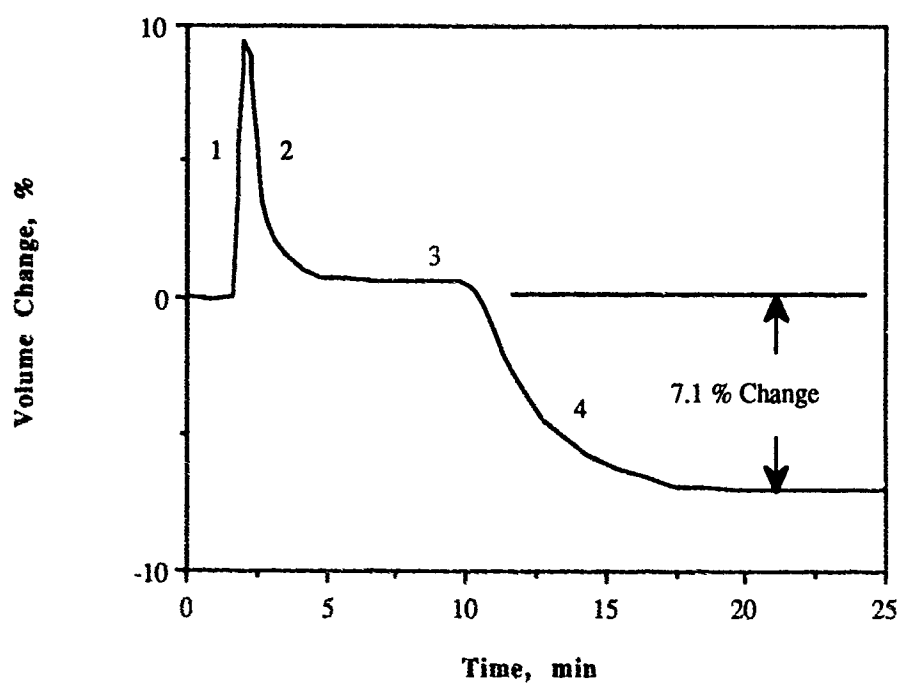


Figure 6. Volume change during cure of a conventional polyester resin. Data from Kroekel and Bartkus²⁴.

condensation reactions)²⁵. A polymer is more dense than its monomer, and the resulting shrinkage upon polymerization can reach 10 to 20 percent²⁶. At point 3, the system has equilibrated after the completion of polymerization. At point 4, thermal contraction is seen as the polymer cools. The volume changes are the basis for kinetic measurements using dilatometry²⁶.

f. Measuring PVT Properties of Polymers

The two methods which can be used to measure PVT properties of samples are the "piston" method and the "confining fluid" method. In the piston method, the sample is placed in a cylinder, and pressure is applied by a piston. Knowing the temperature of the sample, specific volume changes are calculated from the piston displacement. However, one problem with this method is that to avoid leaks, a tight tolerance (10^{-4} cm) must be kept over the entire temperature and pressure range. Another problem is that the piston does not provide a hydrostatic pressure on solid samples, only fluids. In the confining fluid method, the sample is placed in a container with a confining liquid that does not react with the sample. Pressure put on the confining fluid is transferred to the sample. In this case, the specific volume of the sample is calculated from the combined volume changes of the confining fluid and sample¹⁰.

g. Microdielectrometry

Dielectric measurements during composite curing has been described by several investigators²⁷⁻³⁰. The complex dielectric constant describes the polarization response of a material upon the application of an alternating electric field. The permittivity (E1) which is the real part of the complex dielectric constant represents the polarization in phase with the applied electric field. The loss factor (E2) which is the imaginary part of the complex dielectric constant describes the energy dissipation in the sample during polarization. E2 is a function of ionic conductivity. The ionic conductivity is a measure of the motion of ionic impurities in commercial grade resins. Assuming the concentration of the ions is constant, the mobility of ions through the resin is inversely related to the resin viscosity. Therefore, the ionic conductivity, and thus the loss factor, can be correlated with viscosity.

CHAPTER 3

EXPERIMENTAL METHODS

a. Materials

The technique of volumetric dilatometry can be applied to a very broad range of materials. The three class of materials used in this study were thermoplastic polymers, pitch precursor for carbon-carbon composites, and thermoset polymers.

(1) Thermoplastic Polymers

Four thermoplastic polymers were studied: (1) ICI Composite Inc.'s HTA (High Temperature Amorphous), an amorphous thermoplastic described as a biphenyl modified poly(ethersulfone); (2) ICI Composite Inc.'s poly(etheretherketone) (PEEK) 150G, a semicrystalline thermoplastic; (3) ICI Composite Inc.'s HTX, a semicrystalline thermoplastic, chosen because of its different crystallization kinetics than PEEK³¹; and 4) poly-benzobisoxazole (PBO)/PEEK, a random block copolymer with 10 percent wt PBO to 90 percent wt PEEK and unknown block molecular weights and total molecular weights.

(2) Pitch Precursor for Carbon-Carbon Composites

The pitches used were a series of Ashland Oil, Inc. Aerocarb petroleum derived pitches, a Reilly Industries, Inc. Electrode Binder pitch, and a Mitsubishi synthetic pitch. Pitch typically exhibits both "liquid-like" character and "polymer-like" viscoelastic character, depending upon the temperature and strain rate of deformation of the sample. The components of these pitches are generally described as "plate-like" aromatic molecules of 5 to 20 aromatic rings. The pitch will posses a fairly broad molecular weight distribution of components, and this distribution will determine its physical characteristics.

The materials analyzed in this study were Ashland's A-240, A-60, A-70, and A-80, Reilly Industries Electrode Binder Pitch, and Mitsubishi's AR Mesophase Synthetic Pitch. The A-240 system has a carbon content of 50wt percent (as determined by ASTM D-2416) the A-60, A-70, A-80 have carbon contents of 60wt percent, 70wt percent, and 80wt percent, respectively, and the Reilly Coal Pitch has a coking value of 56wt percent. The A-60, A-70, and A-80 are derived from the same feed stock as is the A-240 (carbon percent from vendor's data). Ashland reports a glass transition temperature for these materials, and Reilly reports a softening point for their pitch.

(3) Thermoset Polymers

The materials used in this study were 3501-6 resin, AS4 carbon fiber/3501-6 epoxy tape prepreg, and IM7 carbon fiber/8551-7A toughened epoxy tape prepreg, all from Hercules and IM7 carbon fiber/5250-4 bismaleimide (BMI) 5 harness satin cloth prepreg from BASF. These resins were chosen for their use in the aerospace industry and for the variations in viscosity. Of the three resins, 5250-4 has the lowest viscosity while 8551-7A has the highest. The cure cycle used for each material is listed in Table 1.

b. RDS-II Dynamic Spectrometer

The RDS-II Dynamic Spectrometer from Rheometrics, Inc. was used to determine the elastic and loss modulus of some of the samples. The elastic and loss modulus were measured as a function of temperature at 100 rad/sec frequency and 0.1 percent strain. Each sample was 6.35 cm by 1.27 cm (2.5in by 0.5in) with a layup of $[0^\circ]_{12T}$. In the case of the IM7/5250-4 prepreg cloth, the layup was $[0^\circ/90^\circ]_{3S}$ with the warp was taken to be the 0° direction. HTA and PEEK were heated from -150 to 400°C at a 2°C/min heating rate. Thermoset samples were cured using the cure cycle displayed in Table 1. However, step 1, the pressure application step, was not included. The RDS-II cannot subject the sample to pressure or vacuum.

TABLE 1
CURE CYCLE FOR 3501-6, 8551-7A, AND 5250-4

1. While maintaining 20-29 in Hg vacuum on the bagged layup, pressurize the autoclave to 586 kPa (85 psig).
2. Raise the sample or laminate temperature from room temperature to 116°C (240°F) in 30 minutes.
3. Hold the sample or laminate temperature at 116°C for 60 minutes.
4. Raise the sample or laminate temperature from 116°C to 177°C (350°F) in 25 minutes.
5. Hold the sample or laminate temperature at 177°C for 240 minutes.
6. Cool the sample or laminate to room temperature in 60 minutes.

c. Differential Scanning Calorimetry

Differential Scanning Calorimetry (DSC) was used to find melting points and glass transition points of the pitch samples and the heat of reaction of 5250-4. DSC runs were performed using a DuPont Model 910 DSC. It was controlled with an Omnitherm Advantage [sic] II IBM PS/2-60 data station. The DSC was conducted in air at a flow rate of 20 ml/min. The heating rate was 10°C/min. DSC samples were 5 to 15 mg.

d. Autoclave Cure Monitoring

Laminates were cured from each prepreg using the cure cycle in Table 1. The dimensions were 15.24 cm by 15.24 cm (6in by 6in) with a layup of $[0^\circ]_{12T}$. The IM7/5250-4 layup was as described previously. Each laminate was vacuum debulked overnight before cure. Both a thermocouple and a microdielectrometer placed on each part were used to monitor the temperature and resin flow respectively of the laminates during the cure.

e. PVT Apparatus

(1) Equipment Description

The high pressure volumetric dilatometer used was the Gnomix Research PVT Apparatus. This is a commercial version of an earlier apparatus¹⁰, based on the Bridgman bellows technique³² for the study of liquids which was adapted by Quach and Simha¹¹ to the study of polymers. The PVT apparatus used the confining fluid method to measure PVT properties. The specific volume of polymers can be accurately determined in the 30-400°C temperature range and the 0-200 MPa pressure range. A schematic of the PVT Apparatus is displayed in Figure 7, and a photo is displayed in Figure 8.

The one to two gram sample was enclosed in a piezometer cell (Figure 9), a stainless steel container closed off with flexible metal bellows and filled with mercury (Hg). The piezometer cell was placed in a pressure vessel. Then, a hydrostatic pressure of

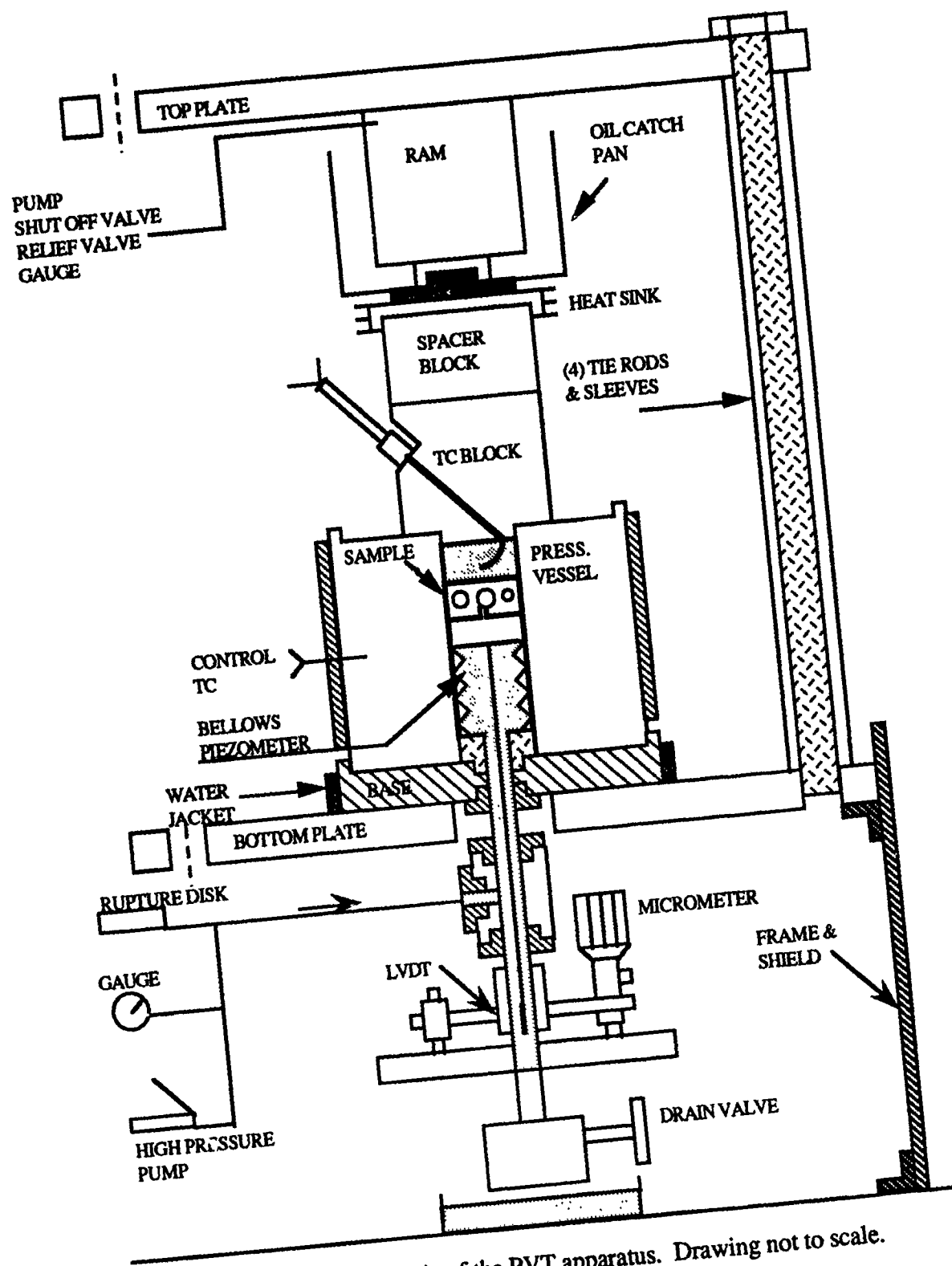


Figure 7. Schematic of the PVT apparatus. Drawing not to scale.

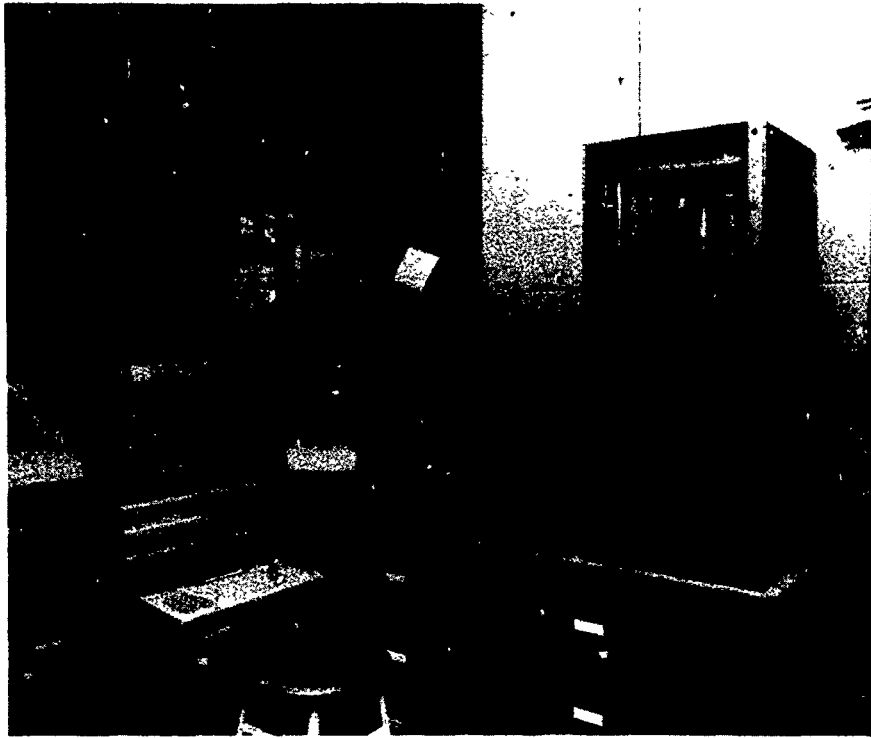


Figure 8. PVT Apparatus with pumps, high-pressure gauge, and associated computer equipment.

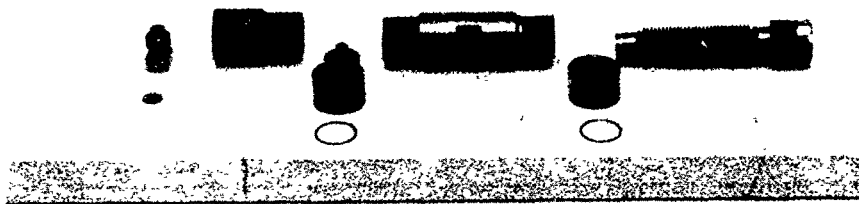


Figure 9. Unassembled piezometer cell.

silicon oil was produced in the vessel by a high-pressure hand pump and was transferred to the contents of the piezometer cell by the bellows. The bellows expanded until the pressure in the vessel equaled the pressure in the cell. The volume change in the polymer was determined through the deflection of the bellows by knowing the effective cross-sectional area of the bellows. A linear variable differential transducer (LVDT) measured the length change of the bellows. The LVDT is accurate to 0.001 mm or 0.001 cm³/g. The LVDT sensitivity was determined by using a precision digital micrometer which is attached to the LVDT coil. The vessel pressure was measured by a high-precision Bourdon gauge.

The temperature in the side of the pressure vessel was measured with a type K thermocouple. Both isothermal holds and temperature ramps were controlled with a Solid-State Relay controller from Omega Engineering, Inc. output to a 1800-watt electrical heater. A separate type K thermocouple was placed close to the sample inside the vessel. The sample temperature and the voltage from the LVDT were read by a DASCON-1 multifunction analog/digital I/O expansion board available from MetraByte Corporation interfaced to a Zenith 248 computer. This information was used by the software available with the PVT apparatus to calculate the change in specific volume with temperature and pressure.

(2) Isothermal Operation

Thermoplastic samples were compressed from 10 to 200 MPa along isotherms from 30°C to 390°C at 20°C intervals. The atmospheric pressure volume of the samples was extrapolated using the Tait equation. The Tait equation is described further in Russell³³. The value for specific volume at atmospheric pressure is extrapolated because Hg boils at 357°C under atmospheric pressure. Any outgassing of Hg or from the sample could produce false volume readings at atmospheric pressure because of the presence of the Hg vapor. Therefore, a minimum pressure of 10 MPa is always maintained on the sample.

(3) Isobaric Operation

Thermoplastic and pitch samples were heated at 2.5°C/min from 30°C to the polymer melt region at constant pressures ranging from 10 to 150 MPa. Then, the samples were cooled at the same pressure through the transition regions. To obtain isobaric data for a material at more than one pressure, a new sample was used at each pressure. The dimensions of each prepreg sample were 1.59 cm by 0.95 cm (5/8in by 3/8in), and the layup was $[0^\circ]_{12T}$. In the case of the IM7/5250-4 cloth, the layup was $[0^\circ/90^\circ]_{3S}$ with the warp was taken to be the 0° direction. All of the thermoset samples were cured using the cure cycle displayed in Table 1. However, step 1, the pressure application step, was not included. Instead, a constant pressure of 10 MPa (1450 psi) was placed on the sample. Volume data were recorded every minute.

CHAPTER 4

THERMOPLASTIC RESULTS

a. HTA

(1) Isothermal Run

The specific volume of HTA is presented in Figure 10 as a function of temperature and pressure during an isothermal scan. The specific volume was measured from 0 to 200 MPa at 10 MPa intervals. For clarity, only isobars at 0, 50, 100, 150, and 200 MPa are shown. At atmospheric pressure, the specific volume changed from 0.7408 cm³/g at 30.2 °C to 0.8157 cm³/g at 388.8°C, corresponding to a 10.1 percent change. At 200 MPa, the specific volume changed from 0.7151 cm³/g at 30.2 °C to 0.7391 cm³/g at 388.8°C, corresponding to a 3.4 percent change. There was a change in slope of the atmospheric pressure PVT curve at 243°C indicating T_g . This T_g value was similar to the value reported by TMA of 248.6°C. However, the T_g value determined from dynamic mechanical analysis (DMA) was 275°C (Figure 11). The T_g value from the DMA data can be affected by the heating rate, measurement frequency, and crystallinity. If a lower frequency than 100 rad/s was used, the T_g value would decrease. At elevated pressures, the glass transition temperature was not as defined as at atmospheric pressure. As discussed in Section 2d, densified glasses form when a polymer in the melt state is compressed. This resulted in "dips" in the isobars where the slope of the isobar deviated from the slope in the glassy region below the atmospheric pressure T_g .

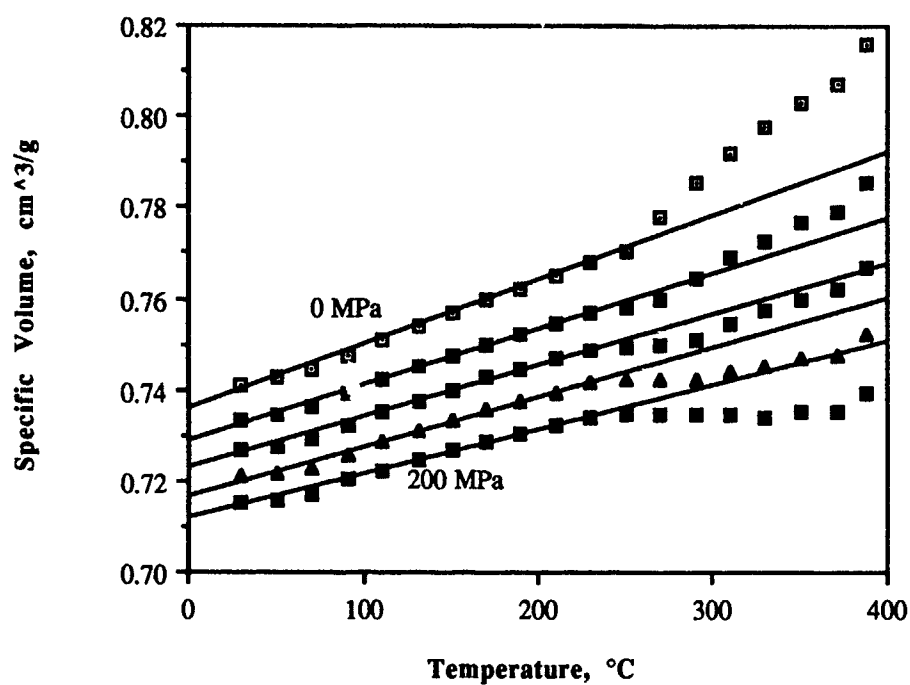


Figure 10. PVT properties of HTA. Selected isobars plotted from isothermal data. Pressures plotted are 0 (top), 50, 100, 150, and 200 MPa (bottom).

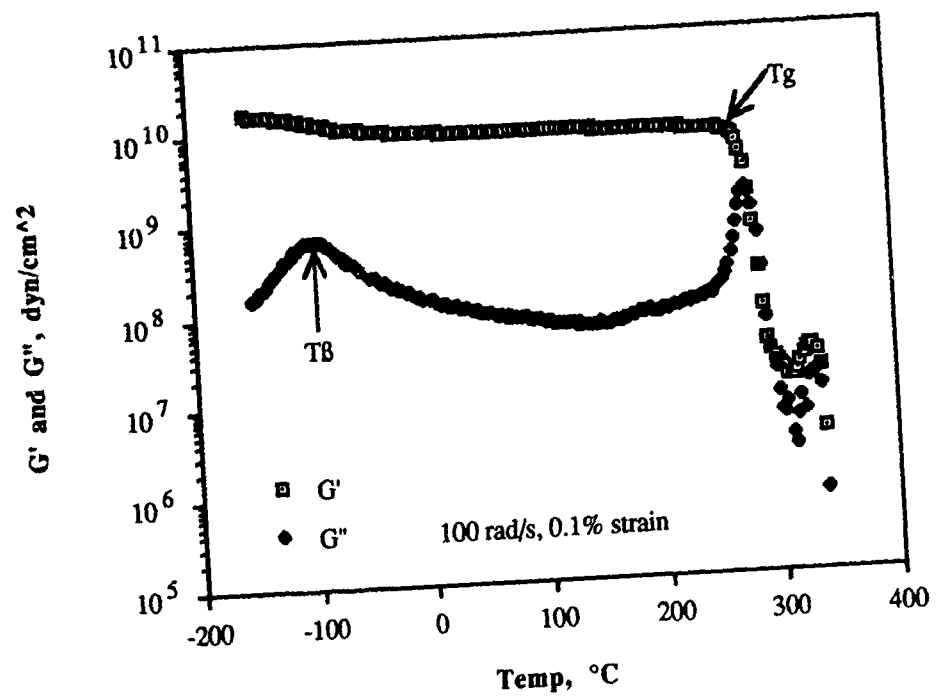


Figure 11. DMA scan of HTA.

(2) Isothermal Pressure Dependence of HTA T_g

At each isobar of the HTA isothermal run (Figure 10), the least squares best fit of the data below the atmospheric pressure T_g was extrapolated to intersect with the isobar at higher temperatures. This intersection is defined as the T_g at that high pressure. Above 120 MPa, this intersection was above the PVT apparatus temperature limit of 400°C; thus, the T_g was only found at pressures below 120 MPa. The HTA T_g dependence on pressure from isothermal data is displayed in Figure 12. Two linear relationships with similar slopes were found:

$$T_g(P) = 0.81733 P + 248.17; P \leq 80 \text{ MPa} \quad (1)$$

$$T_g(P) = 0.82600 P + 303.02; P \geq 80 \text{ MPa} \quad (2)$$

At 80 MPa, there appeared to be two points where the data intersected the low temperature best fit line: one near 310°C and one near 370°C (Figure 13). Above 80 MPa, only one intersection point occurred, but it was shifted to a higher temperature (Figure 14). It was difficult to define the intersection temperature at 80 MPa because of the shape of the curve at the higher temperatures. The volumes appeared to follow the slope of the low temperature data but are shifted below the extrapolated line (see Figure 14). The similar slopes of equations 1 and 2 indicated that the data follows the same general trend, while the different intercepts resulted from the problem in finding T_g at the higher pressures.

(3) Thermal Expansion of HTA

The polymer specific volume along isobars below the atmospheric pressure T_g was fit to the equations:

$$V(P,T) = m(P) T + b(P) \quad (3)$$

$$V(P,T) = a(P) \exp(\alpha(P) T) \quad (4)$$

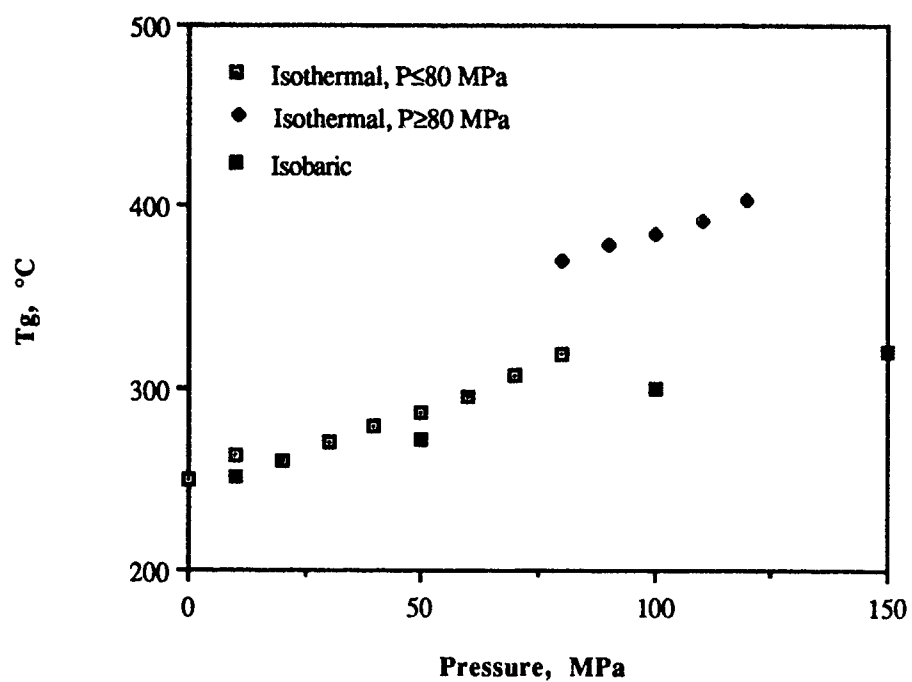


Figure 12. Isothermal and isobaric dependence of the HTA T_g on pressure.

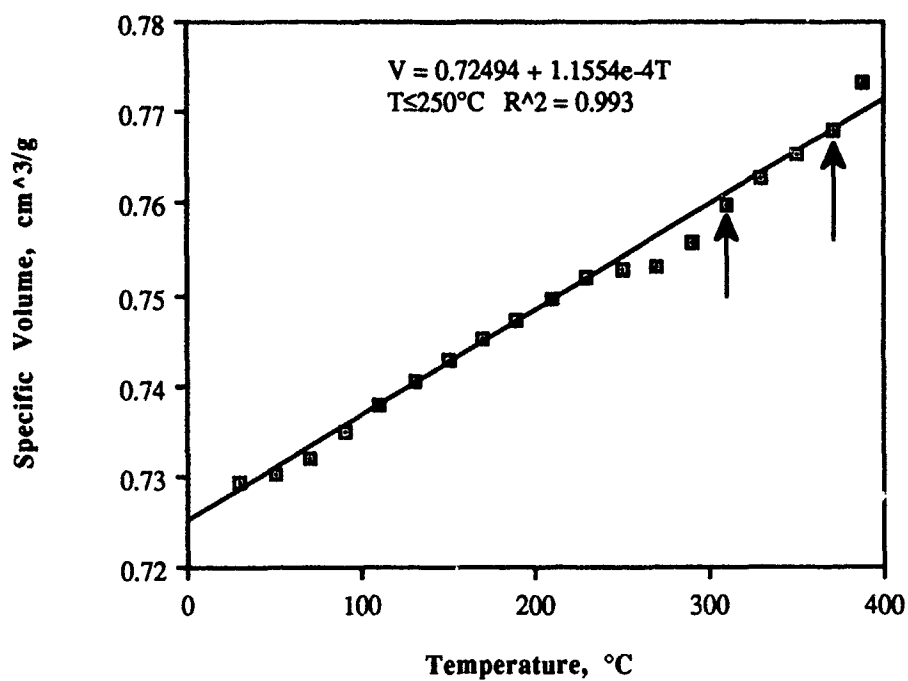


Figure 13. PVT properties of HTA at 80 MPa from isothermal data. Arrows indicate possible T_g values.

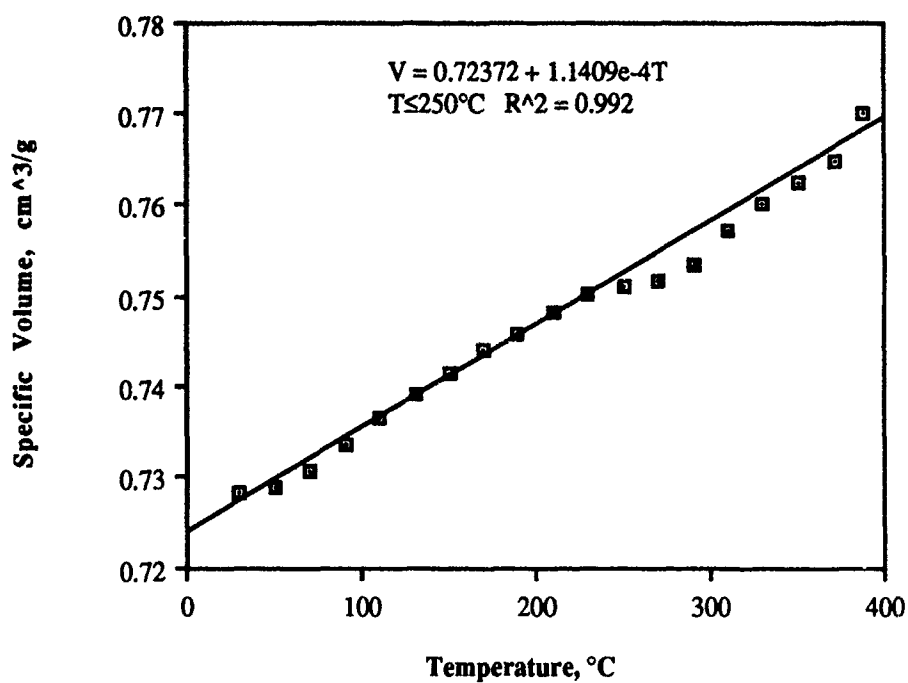


Figure 14. PVT properties of HTA at 90 MPa from isothermal data.

where V is the specific volume in cm^3/g , P is the pressure in MPa, T is the temperature in degrees Centigrade, m is the slope in $\text{cm}^3/\text{g } ^\circ\text{C}$, b is the y-intercept in cm^3/g , α is the coefficient of thermal expansion (CTE) in $1/^\circ\text{C}$, and a is the intercept in cm^3/g . Data were not fit above the atmospheric pressure T_g because of the increasing curvature in the data. Table 2 lists the coefficients for HTA. The dependence of CTE on pressure is displayed in Figure 15. CTE decreases as pressure increases. As pressure increases, molecular motions should become more restricted, thus decreasing thermal expansion.

(4) HTA Isobaric Runs

(a) Isobaric Pressure Dependence of HTA T_g . The isobaric data for HTA is displayed in Figure 16. The pressure dependence of T_g is defined as it was in Section 4a(2). The HTA T_g dependence on pressure from isobaric data is displayed in Figure 11. The equation for isobaric pressure dependence of T_g during heating is:

$$T_g(P) = 0.50158 P + 246.63 \quad (5)$$

The T_g values during cooling were similar to the heating values. The slope of Equation 5 describing isobaric pressure dependence on T_g is smaller than the slope of Equations 1 and 2 for the isothermal pressure dependence of T_g . Also, the values of T_g for isobaric runs were lower than the isothermal values at the same pressures. T_g is dependent on the temperature and pressure history; therefore, the different thermal and pressure histories for the isobaric and isothermal runs affected the T_g .

(b) Densification of HTA During Pressurized Cooling. At each pressure, the specific volume measured during cooling was slightly less than the volume measured during heating. This would be expected because the samples were originally formed at much lower pressures than the pressures applied during cooling. The higher forming

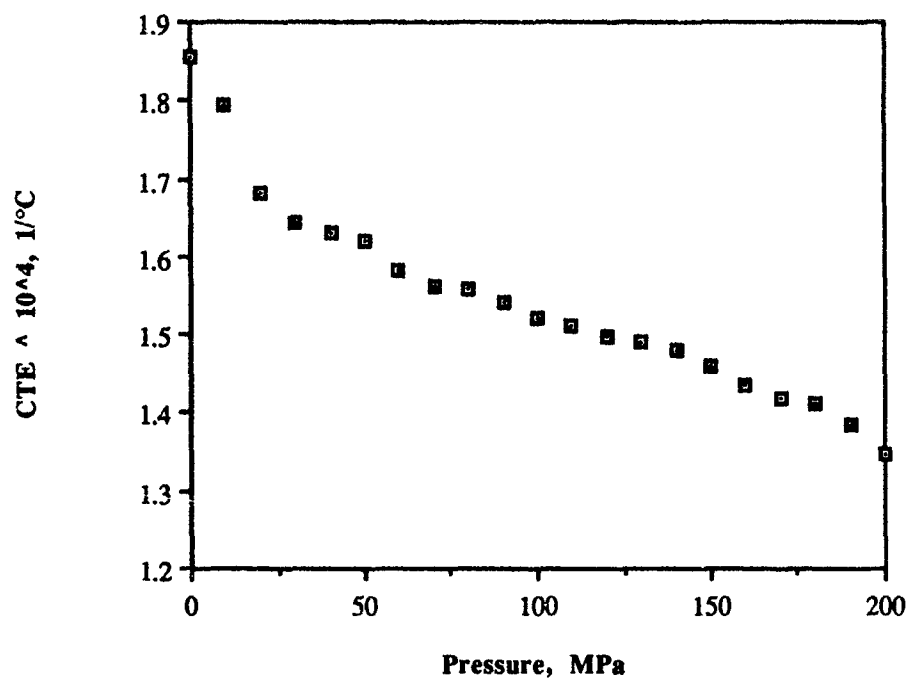


Figure 15. CTE dependence on pressure of HTA.

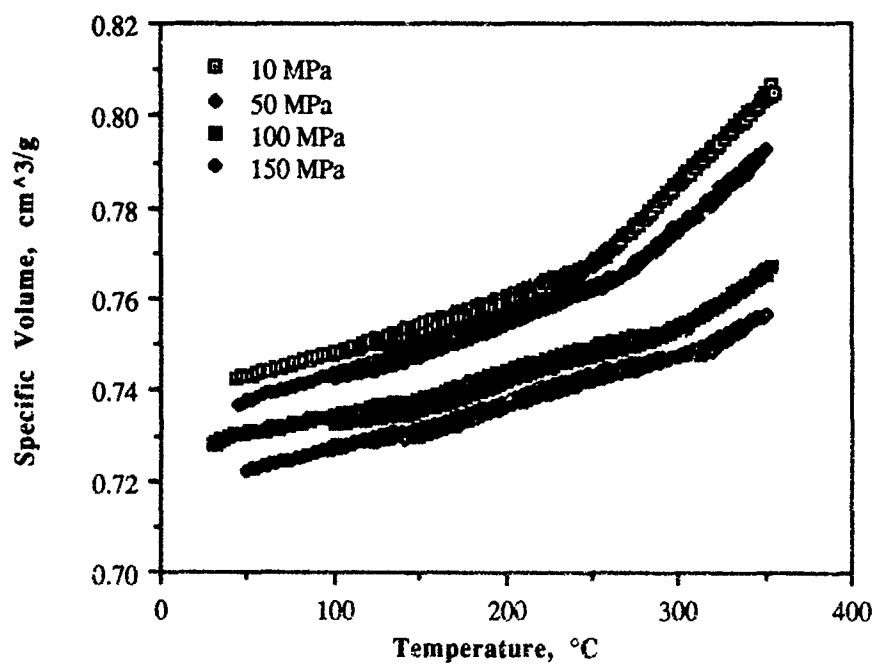


Figure 16. Isobaric runs of HTA at 10, 50, 100, and 150 MPa.

TABLE 2
COEFFICIENTS OF THE VOLUME-TEMPERATURE EQUATIONS
FOR THE GLASSY REGION OF HTA
(temperature range 30 to 250°C)

P (MPa)	$m \times 10^4$ ($\text{cm}^3/\text{g } ^\circ\text{C}$)	b (cm^3/g)	$\alpha \times 10^4$ ($1/^\circ\text{C}$)	a (cm^3/g)
0	1.4011	0.73545	1.8552	0.73565
10	1.3500	0.73414	1.7925	0.73432
20	1.2613	0.73311	1.6802	0.73326
30	1.2310	0.73178	1.6438	0.73192
40	1.2186	0.73031	1.6311	0.73045
50	1.2086	0.72879	1.6212	0.72894
60	1.1766	0.72762	1.5817	0.72775
70	1.1631	0.72630	1.5606	0.72643
80	1.1554	0.72494	1.5594	0.72507
90	1.1409	0.72372	1.5428	0.72384
100	1.1231	0.72257	1.5216	0.72269
110	1.1122	0.72131	1.5097	0.72143
120	1.1002	0.72015	1.4961	0.72027
130	1.0935	0.71896	1.4896	0.71907
140	1.0841	0.71771	1.4795	0.71782
150	1.0676	0.71667	1.4596	0.71678
160	1.0480	0.71562	1.4355	0.71572
170	1.0344	0.71449	1.4195	0.71459
180	1.0264	0.71339	1.4106	0.71349
190	1.0058	0.71236	1.3849	0.71246
200	0.9753	0.71152	1.3453	0.71161

pressures in the dilatometer collapsed more free volume in the polymer than the original forming pressures did, thus creating a denser material.

b. PEEK

(1) PEEK Isothermal Run

The specific volume of PEEK as a function of temperature and pressure during an isothermal scan is displayed in Figure 17. As with HTA, the specific volume was measured from 0 to 200 MPa at 10 MPa intervals. For visual clarity, only isobars at 0, 100, and 200 MPa are shown. At atmospheric pressure, the specific volume changed from 0.7547 cm³/g at 30.0 °C to 0.9129 cm³/g at 386.1°C, corresponding to a 21.0 percent change. At 200 MPa, the specific volume changed from 0.7323 cm³/g at 30.2 °C to 0.8086 cm³/g at 388.8°C, corresponding to a 10.4 percent change. The change in specific volume of PEEK was greater than the change in specific volume of HTA because of the crystallinity in PEEK. The T_g indicated by the change in slope in the atmospheric pressure isobar was near 150°C. The DMA reported T_g value is 148°C (Figure 18). As with HTA, dips in the isobars at higher pressures were present for PEEK. This indicated that the amorphous part of the PEEK resin also becomes a densified glass when pressurized from the melt state. This phenomenon was also seen by Zoller et al.¹⁸, who stated that the amorphous region in PEEK thermodynamically behaves like pure amorphous polymers because the PEEK polymer chains have greater conformational freedom from the presence of crystals than other semicrystalline materials.

The end of the melting region of PEEK indicated by the sharp break in the atmospheric pressure isobar was near 350°C. The DMA data indicated melting in the same region. The temperature of the end of the melting region increased with pressure. However, as indicated by Zoller et al.¹⁸, isothermal runs do not determine melting point pressure dependence because the thermodynamic equilibrium is competing with crystallization kinetics.

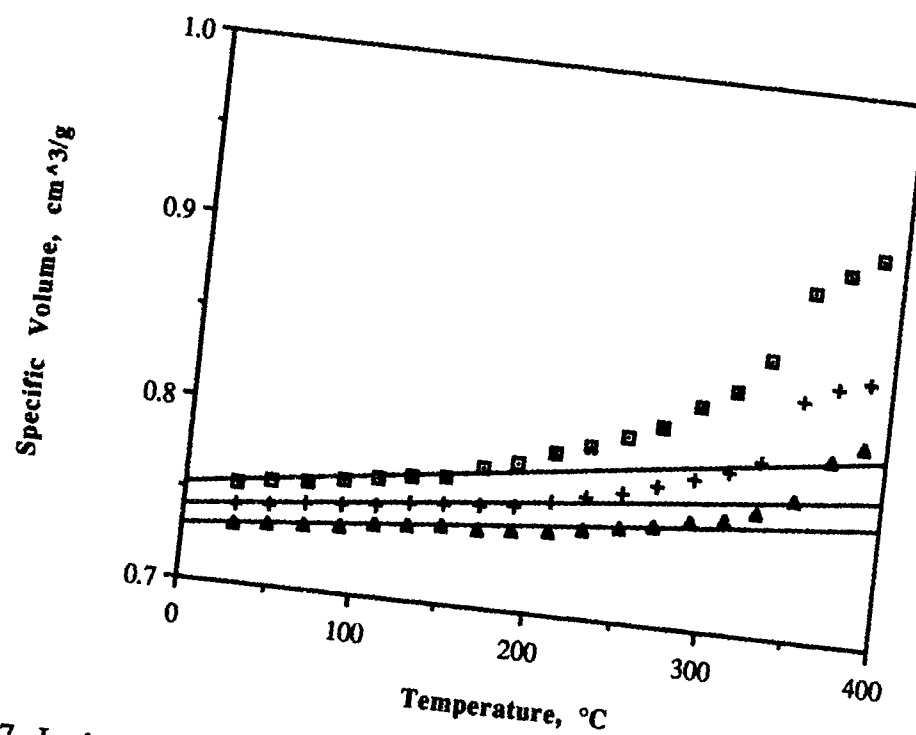


Figure 17. Isothermal PVT properties of PEEK. Selected isobars plotted from isothermal data. Pressures plotted are 0 (top), 100, and 200 MPa (bottom).

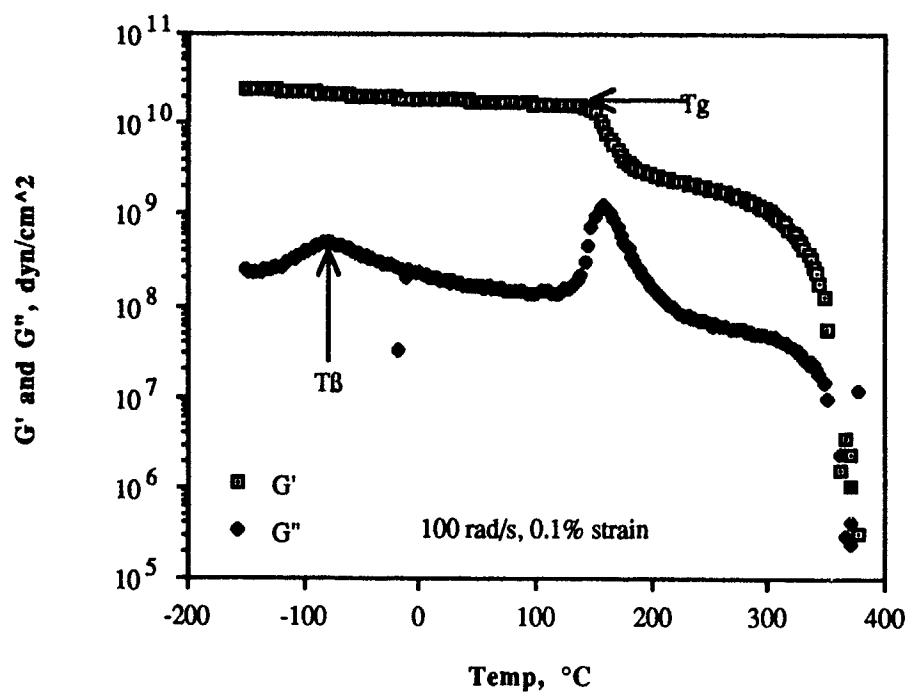


Figure 18. DMA scan of PEEK.

(2) Isothermal Pressure Dependence of PEEK T_g

The pressure dependence of T_g for PEEK from isothermal data is displayed in Figure 19 and can be represented by:

$$T_g(P) = 0.52379 P + 145.24 \quad (6)$$

for $P \geq 40$ MPa. $T_g(P)$ at 10, 20, and 30 MPa was not obtained because the dips in the data were not seen at these pressures. The T_g values for these pressures were still near 150°C . Therefore, these data were not used in obtaining the relationship. This equation agreed with the equation found by Zoller et al.¹⁸ for isothermal data:

$$T_g(P) = 0.574 P + 152.0 \quad (7)$$

(3) Thermal Expansion of PEEK

Again, the polymer specific volume along isobars below the atmospheric pressure T_g was fit to Equations 3 and 4. Data was not fit above the atmospheric pressure T_g because of the increasing curvature in the data. Also, the data above the melting point were not fit. Table 3 lists the coefficients for PEEK. Both equations fit the experimental data well. In addition, the experimentally determined coefficients for PEEK agreed with the coefficients found by Zoller, et. al.¹⁸. The dependence of CTE on pressure is displayed in Figure 20.

(4) PEEK Isobaric Runs

(a) Isobaric Pressure Dependence of T_g . The isobaric data for PEEK is displayed in Figure III-12. The pressure dependence of T_g is defined as it was in section 4a(2). The equation for isobaric pressure dependence of T_g during heating is:

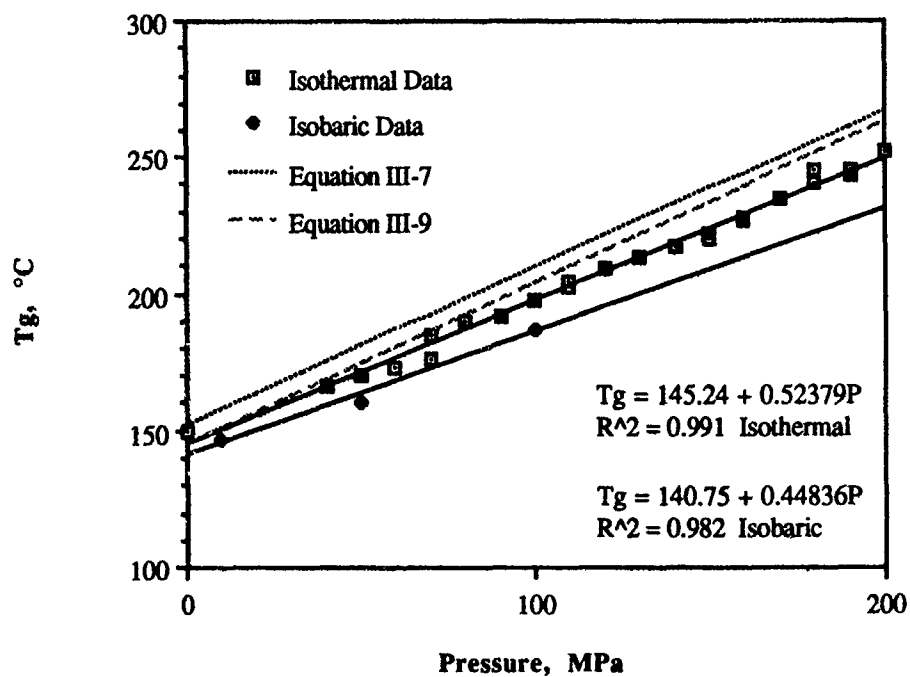


Figure 19. Dependence of the PEEK T_g on pressure from isothermal and isobaric data.

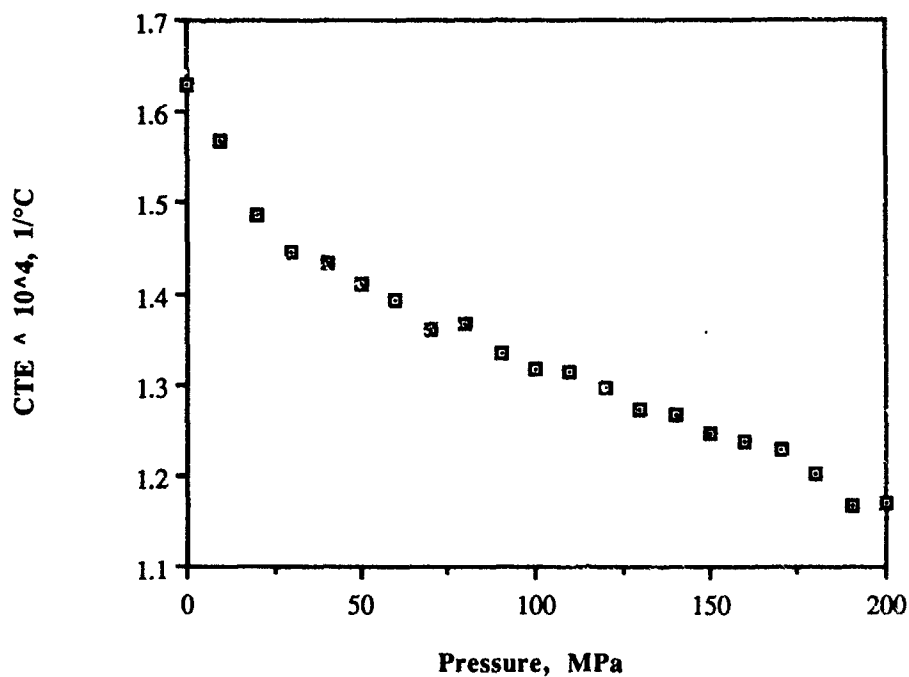


Figure 20. Pressure dependence of CTE for PEEK.

TABLE 3
COEFFICIENTS OF THE VOLUME-TEMPERATURE EQUATIONS
FOR THE GLASSY REGION OF PEEK
(temperature range 30 to 250°C)

P (MPa)	$m \times 10^4$ ($\text{cm}^3/\text{g } ^\circ\text{C}$)	b (cm^3/g)	$\alpha \times 10^4$ ($1/^\circ\text{C}$)	a (cm^3/g)
0	1.2420	0.75057	1.6301	0.75064
10	1.1917	0.74949	1.5673	0.74956
20	1.1272	0.74847	1.4858	0.74853
30	1.0948	0.74732	1.4458	0.74737
40	1.0840	0.74610	1.4342	0.74616
50	1.0644	0.74491	1.4107	0.74496
60	1.0482	0.74378	1.3916	0.74383
70	1.0229	0.74271	1.3604	0.74275
80	1.0266	0.74158	1.3674	0.74162
90	0.9997	0.74058	1.3337	0.74062
100	0.9853	0.73952	1.3166	0.73956
110	0.9817	0.73828	1.3140	0.73832
120	0.9673	0.73732	1.2966	0.73737
130	0.9475	0.73633	1.2721	0.73637
140	0.9421	0.73526	1.2667	0.73530
150	0.9259	0.73434	1.2467	0.73438
160	0.9187	0.73332	1.2388	0.73335
170	0.9096	0.73229	1.2282	0.73233
180	0.8898	0.73148	1.2032	0.73151
190	0.8611	0.73055	1.1663	0.73058
200	0.8628	0.72953	1.1701	0.72957

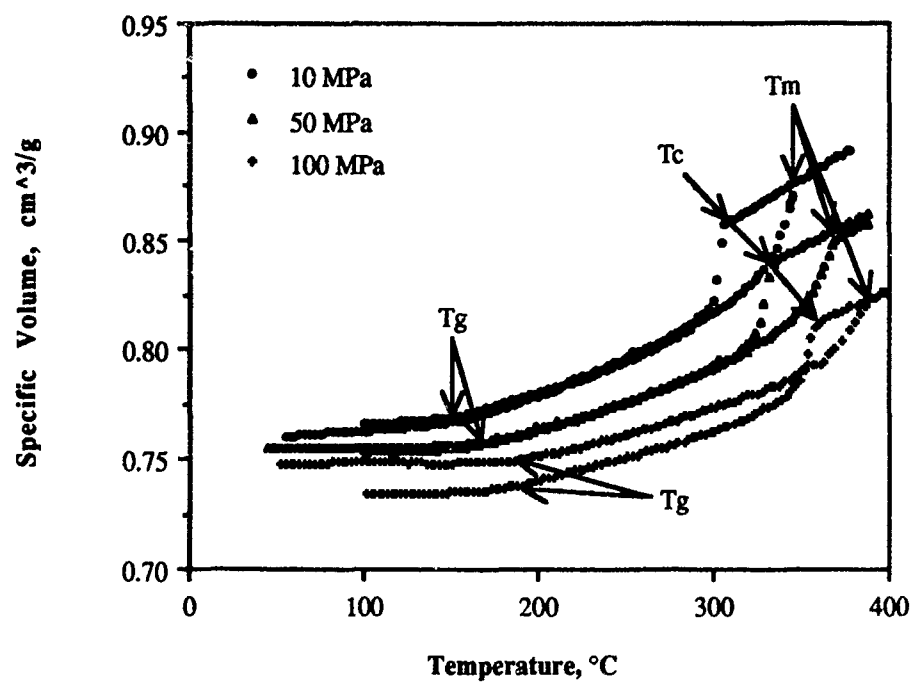


Figure 21. Isobaric runs of PEEK at 10, 50, and 100 MPa.

$$T_g(P) = 0.44836 P + 140.75 \quad (8)$$

As with HTA, the T_g values during cooling were similar to the heating values. The equations describing the isobaric and pressure dependence of T_g were different from the equations found by Zoller et al.¹⁸:

$$T_g(P) = 0.59 P + 144.6 \quad (9)$$

However, Zoller et al.¹⁸ used 380 grade PEEK while 150 grade PEEK was used in this study. The 150 grade PEEK has a lower molecular weight than 380 grade PEEK. Also, the slope of equation III-8 is different than the slope of Equation 6, the isothermal pressure dependence of T_g . As with HTA, the values of T_g for isobaric runs of PEEK were lower than the isothermal values at the same pressures. T_g is dependent on the temperature and pressure history. Therefore, the different thermal and pressure histories for the isobaric and isothermal runs changed the T_g measurement.

(b) Densification During Pressurized Cooling. For PEEK at 10 MPa, the volumes measured during cooling were slightly greater than the volumes measured during heating. At 50 MPa, the volumes measured during cooling were slightly less than the volumes measured during heating. At 100 MPa, the volumes measured during cooling were much less than the volumes measured during heating. This large volume change may have occurred because the high pressure caused increased crystallinity in PEEK sample and therefore increased density compared to the crystallinity in the sample when it was originally formed at 68.9 kPa (10 psi).

(c) Melting and Crystallization of PEEK. The melting and crystallization curves (Figure 21) shifted to higher temperatures as pressure increased. The melting temperature (T_m) is the temperature at which the heating curve slope changes from steep to shallow. The crystallization temperature (T_c) is the temperature at which the cooling curve slope changes

from shallow to steep. T_c is less than T_m because PEEK undergoes supercooling before crystallization. The pressure dependence of T_m and T_c is displayed in Figure III-13. The equations describing the relationship between T_m , T_c , and P are:

$$T_m = 344.4 + 0.443 P \quad (9)$$

$$T_c = 302.0 + 0.600 P \quad (10)$$

At $P = 0$, the melting point found by Equation 9 corresponded to DSC measurements of $T_m = 344^\circ\text{C}$ ¹. The crystallization point of 308°C measured by DSC³¹ agreed with the temperature calculated using Equation 10. The relations found for T_m and T_c were different than found by Zoller et al.¹⁸:

$$T_m = 338.4 + 0.483 P \quad (11)$$

$$T_c = 300.8 + 0.512 P \quad (12)$$

The volume change from 400 to 30°C was also different. However, Zoller et al. used 380 grade PEEK, while 150 grade PEEK was used in this study. The 150 grade PEEK has a lower molecular weight than 380 grade PEEK.

c. HTX

(1) Isothermal Run

The isothermal PVT properties of HTX are displayed in Figure 23. Again, the specific volume was measured from 0 to 200 MPa at 10 MPa intervals. For visual clarity, only isobars at 0, 100, and 200 MPa are shown. At atmospheric pressure, the specific volume changed from $0.7541 \text{ cm}^3/\text{g}$ at 30.2°C to $0.8801 \text{ cm}^3/\text{g}$ at 386.9°C , corresponding to a 16.7 percent change. At 200 MPa, the specific volume changed from

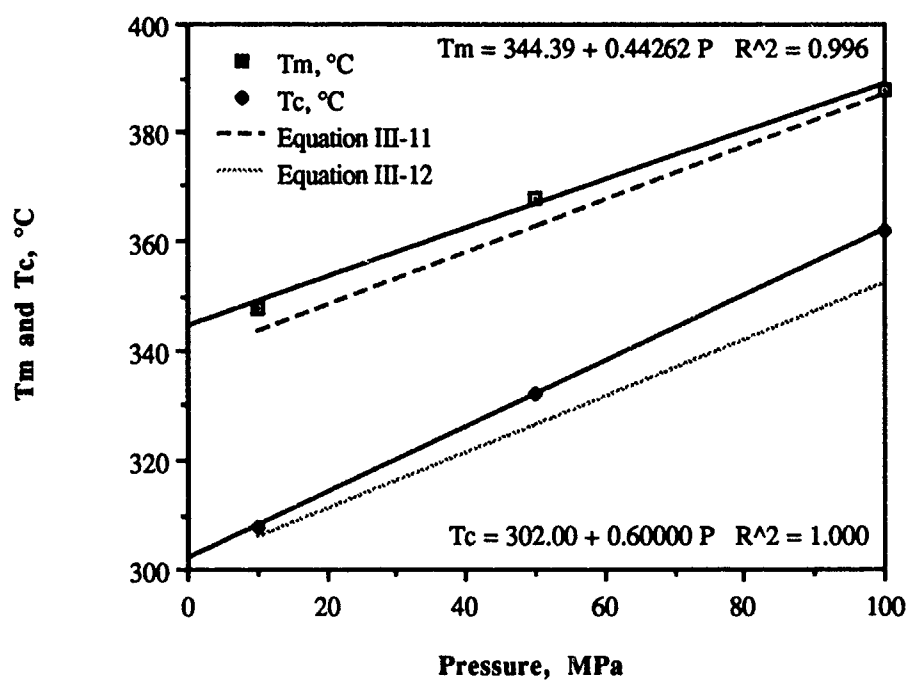


Figure 22. Isobaric pressure dependence of T_m and T_c for PEEK.

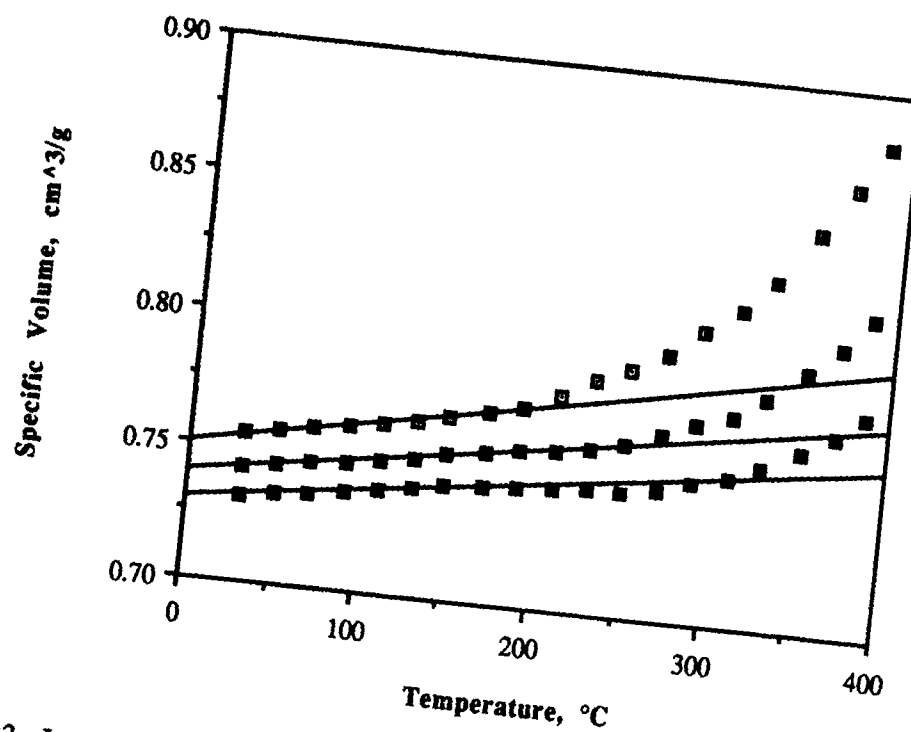


Figure 23. Isothermal PVT properties of HTX. Selected isobars plotted from isothermal data. Pressures plotted are 0 (top), 100, and 200 MPa (bottom).

0.7315 cm³/g at 30.6 °C to 0.7809 cm³/g at 386.9°C, corresponding to a 6.8 percent change. There was a change in slope of the atmospheric PVT curve near 200°C indicating T_g . This T_g value was similar to the value reported by Anderson³¹. Again, this resulted in "dips" in the isobars above the atmospheric pressure T_g at elevated pressures.

Anderson³¹ reports that DSC scans of HTX show two melting peaks, one at 373°C and one at 405°C. The PVT data do show a steadily increasing volume-temperature slope as the temperature increases. However, a clearly defined melting point as seen with PEEK is not seen with HTX because the maximum temperature of the PVT apparatus is 400°C, below the final melting point of HTX.

(2) Isothermal Pressure Dependence of HTX T_g

The pressure dependence of T_g for HTX from isothermal data is displayed in Figure 24 and can be represented by:

$$T_g(P) = 148.72 + 1.1145 P - 0.0017687 P^2 \quad (13)$$

This equation is only valid in the range $60 \text{ MPa} \leq P \leq 200 \text{ MPa}$. $T_g(P)$ from 10 to 50 MPa was not obtained because the data did not dip significantly from linearity above the atmospheric pressure, T_g . Furthermore, the $T_g(P)$ from 10 to 50 MPa does not increase from the atmospheric pressure T_g of 200°C. As a result, these data were not used in obtaining the relationship.

(3) Thermal Expansion of HTX

Again, the polymer specific volume along isobars below the atmospheric pressure T_g was fit to Equations 3 and 4. Data were not fit above the atmospheric pressure, T_g , because of the increasing curvature in the data. Also, the data above the melting point were not fit. Table 4 lists the coefficients for HTX. The dependence of CTE on pressure is displayed in Figure 25.

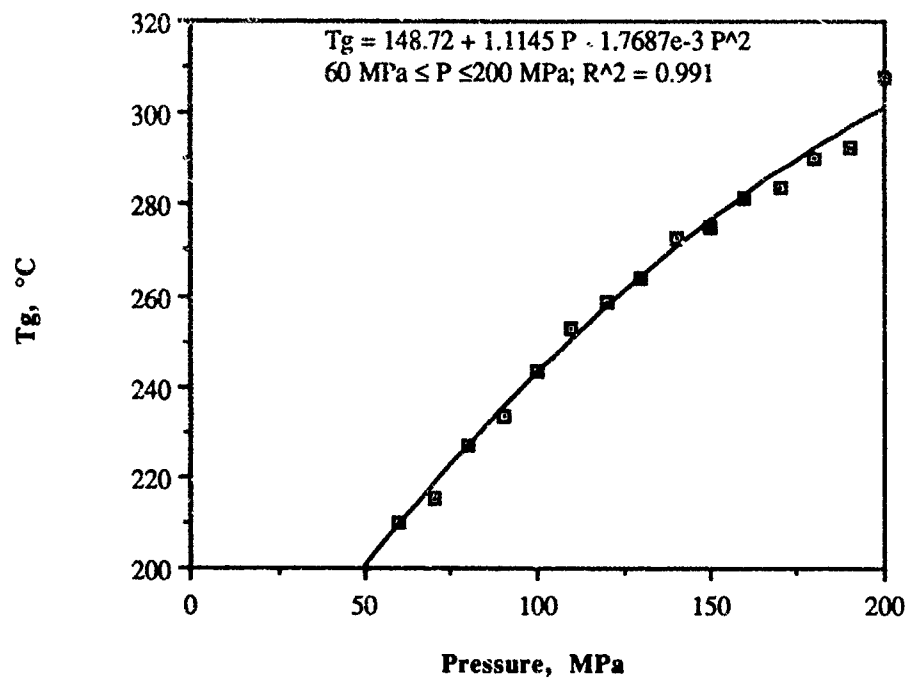


Figure 24. Pressure dependence of the HTX T_g on isothermal data.

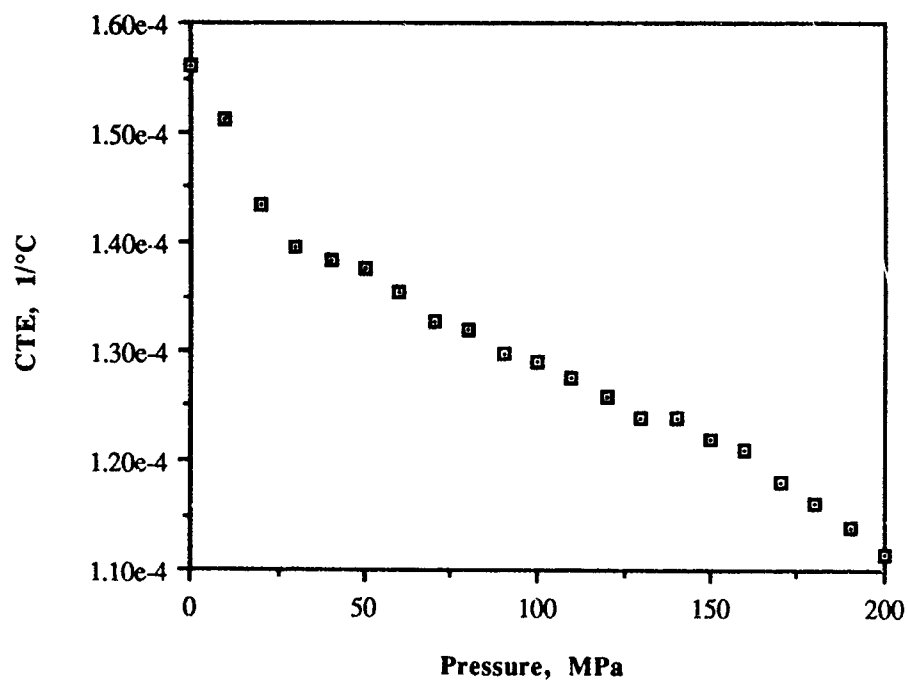


Figure 25. Pressure dependence of the HTX CTE.

TABLE 4
COEFFICIENTS OF THE VOLUME-TEMPERATURE EQUATIONS
FOR THE GLASSY REGION OF HTX
(temperature range 30 to 200°C)

Pressure (MPa)	m, (cm ³ /g °C)	b (cm ³ /g)	alpha (1/°C)	a (cm ³ /g)
0	1.1912E-04	0.74996	1.5603E-04	0.75005
10	1.1528E-04	0.74882	1.5132E-04	0.74891
20	1.0904E-04	0.74785	1.4346E-04	0.74793
30	1.0590E-04	0.74677	1.3960E-04	0.74684
40	1.0468E-04	0.74553	1.3824E-04	0.74560
50	1.0391E-04	0.74426	1.3747E-04	0.74433
60	1.0205E-04	0.74314	1.3526E-04	0.74321
70	9.9982E-05	0.74208	1.3273E-04	0.74214
80	9.9206E-05	0.74090	1.3193E-04	0.74096
90	9.7483E-05	0.73988	1.2985E-04	0.73994
100	9.6793E-05	0.73871	1.2914E-04	0.73877
110	9.5503E-05	0.73763	1.2763E-04	0.73768
120	9.4011E-05	0.73663	1.2584E-04	0.73669
130	9.2475E-05	0.73566	1.2397E-04	0.73572
140	9.2318E-05	0.73447	1.2397E-04	0.73453
150	9.0640E-05	0.73355	1.2191E-04	0.73360
160	8.9842E-05	0.73251	1.2102E-04	0.73256
170	8.7510E-05	0.73170	1.1805E-04	0.73175
180	8.5905E-05	0.73074	1.1606E-04	0.73079
190	8.4258E-05	0.72983	1.1401E-04	0.73017
200	8.2339E-05	0.72891	1.1158E-04	0.72895

d. PBO/PEEK

(1) Isothermal Run

The isothermal PVT properties of PBO/PEEK are displayed in Figure 26. The specific volume was measured from 0 to 200 MPa at 10 MPa intervals. For visual clarity, only isobars at 0, 100, and 200 MPa are shown. At atmospheric pressure, the specific volume changed from 0.7539 cm³/g at 30.2°C to 0.9164 cm³/g at 387.3°C, corresponding to a 21.6 percent change. At 200 MPa, the specific volume changed from 0.7315 cm³/g at 30.2 °C to 0.8117 cm³/g at 387.3°C, corresponding to a 11.0 percent change. There was a change in slope of the atmospheric PVT curve near 140°C indicating T_g. This result disagrees with the T_g value reported by Dow Chemical of 160°C³⁴. At elevated pressures, densified glasses begin to form along the 150°C isotherm. This indicates that the polymer was in the melt state and pressurized back into a glass. Therefore, the T_g cannot be 160°C.

The atmospheric pressure melting point of PBO/PEEK indicated by the sharp break in the atmospheric pressure isobar was near 350°C. Dow Chemical also reported the melting point around 350°C³⁴. As with PEEK, the melting temperature increased with pressure. However, as indicated by Zoller et al.¹⁸, isothermal runs do not determine melting point pressure dependence of semicrystalline polymers because the thermodynamic equilibrium is competing with crystallization kinetics.

(2) Isothermal Pressure Dependence of PBO/PEEK T_g

The pressure dependence of T_g for PBO/PEEK from isothermal data is displayed in Figure 27 and can be represented by:

$$T_g(P) = 102.29 + 1.5814 P - 8.1575E-3 P^2 + 2.0528E-5 P^3 \quad (13)$$

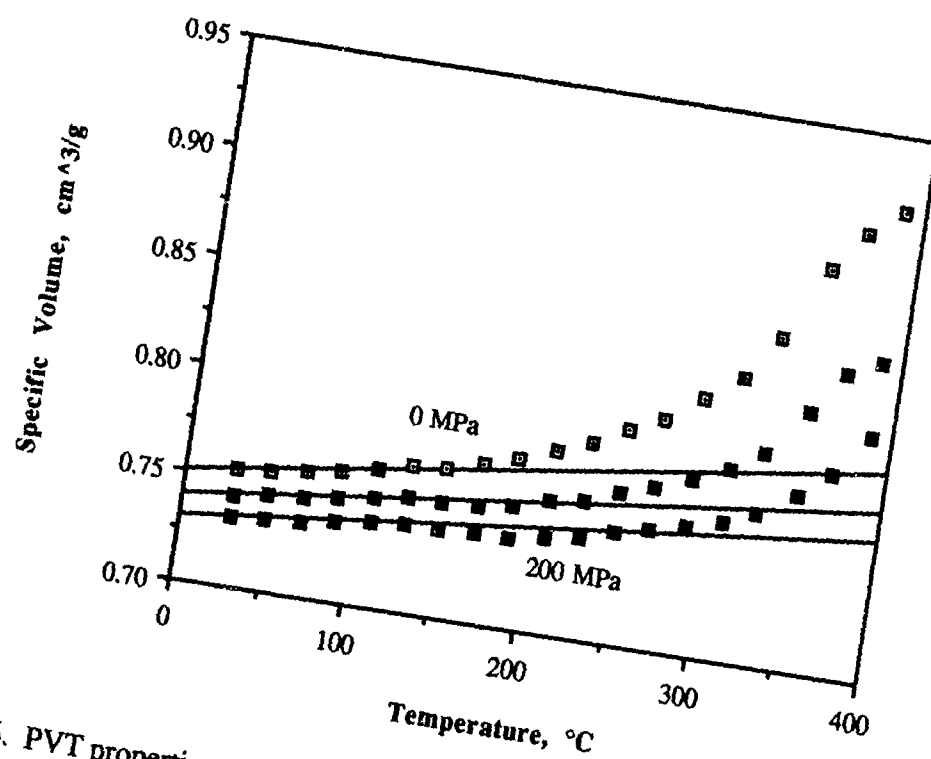


Figure 26. PVT properties of PBO/PEEK. Selected isobars plotted from isothermal data. Pressures plotted are 0 (top), 100, and 200 MPa (bottom).

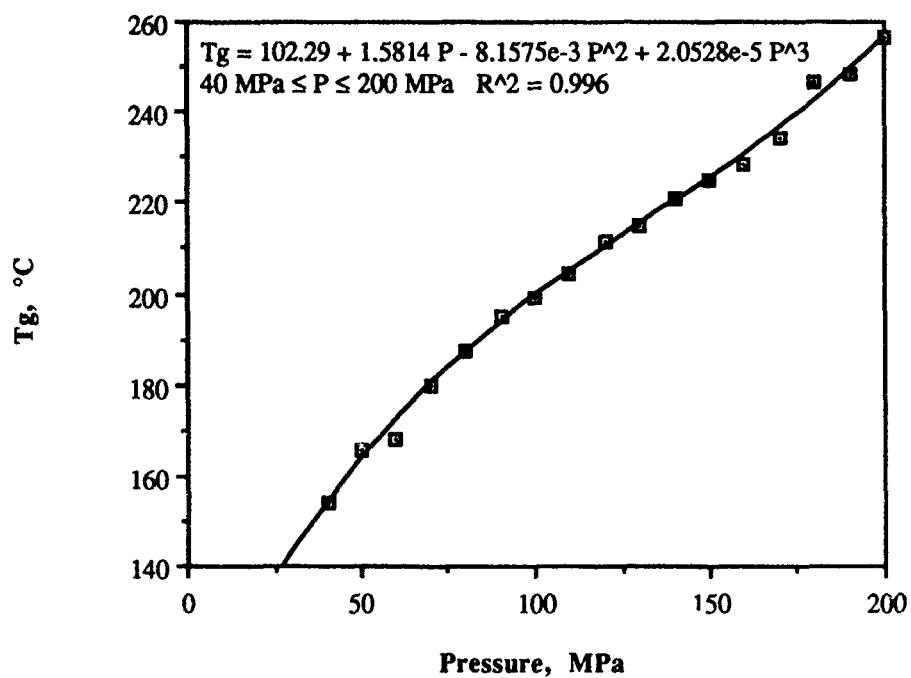


Figure 27. Pressure dependence of the PBO/PEEK T_g on isothermal data.

This equation is only valid in the range $40 \text{ MPa} \leq P \leq 200 \text{ MPa}$. $T_g(P)$ from 10 to 30 MPa was not obtained because the data did not dip significantly from linearity above the atmospheric pressure T_g . Furthermore, the $T_g(P)$ from 10 to 30 MPa was still near the atmospheric pressure T_g of 140°C . As a result, these data were not used in obtaining the relationship.

(3) Thermal Expansion of PBO/PEEK

Again, the polymer specific volume along isobars below the atmospheric pressure, T_g was fit to Equations 3 and 4. Data were not fit above the atmospheric pressure, T_g , because of the increasing curvature in the data. Also, the data above the melting point were not fit. Table 5 lists the coefficients for PBO/PEEK. Both equations fit the experimental data well. The dependence of CTE on pressure is displayed in Figure 28.

e. Conclusions

PVT properties of amorphous and semicrystalline thermoplastic polymers were found. Both isothermal and isobaric runs were made on the materials. Glass transition, melting, and recrystallization could be seen from these data. Each of the three phenomena as well as the coefficient of thermal expansion of each polymer increased with increasing pressure. T_g measured in isobaric runs was slightly less than the T_g measured in isothermal runs. In isothermal runs, densified glasses formed when a polymer in the melt state is compressed. This resulted in "dips" in the isobars where the slope of the isobar deviated from the slope in the glassy region below the atmospheric pressure, T_g . In isobaric runs, densified glasses were also formed during cooldown from the melt state at high pressure. Large amounts of shrinkage while cooling PEEK under high pressures may induce additional crystallization. It is difficult to obtain a relationship between pressure and T_g at low pressures for isothermal runs. The relationship of pressure and T_g at higher pressures for isothermal runs is similar to the relationship for isobaric runs. However at lower

TABLE 5
COEFFICIENTS OF THE VOLUME-TEMPERATURE EQUATIONS
FOR THE GLASSY REGION OF PBO/PEEK
(temperature range 30 to 130°C)

<u>P</u> (MPa)	<u>m</u> (cm ³ /g °C)	<u>b</u> (cm ³ /g)	<u>alpha</u> (1/°C)	<u>a</u> (cm ³ /g)
0	1.1786E-04	0.74988	1.5539E-04	0.74992
10	1.1366E-04	0.74874	1.5015E-04	0.74878
20	1.0539E-04	0.74781	1.3950E-04	0.74784
30	1.0376E-04	0.74659	1.3759E-04	0.74663
40	1.0288E-04	0.74529	1.3665E-04	0.74532
50	1.0089E-04	0.74413	1.3423E-04	0.74416
60	9.7267E-05	0.74312	1.2964E-04	0.74315
70	9.9635E-05	0.74171	1.3301E-04	0.74174
80	9.7330E-05	0.74076	1.3014E-04	0.74080
90	9.6526E-05	0.73962	1.2927E-04	0.73964
100	9.6146E-05	0.73853	1.2894E-04	0.73856
110	9.5157E-05	0.73747	1.2780E-04	0.73750
120	9.3903E-05	0.73651	1.2630E-04	0.73654
130	8.9522E-05	0.73575	1.2057E-04	0.73578
140	9.0333E-05	0.73459	1.2184E-04	0.73461
150	8.8719E-05	0.73365	1.1982E-04	0.73368
160	8.7128E-05	0.73272	1.1784E-04	0.73274
170	8.3729E-05	0.73201	1.1339E-04	0.73203
180	8.8496E-05	0.73059	1.2004E-04	0.73061
190	8.6217E-05	0.72971	1.1712E-04	0.72974
200	8.6896E-05	0.72871	1.1820E-04	0.72873

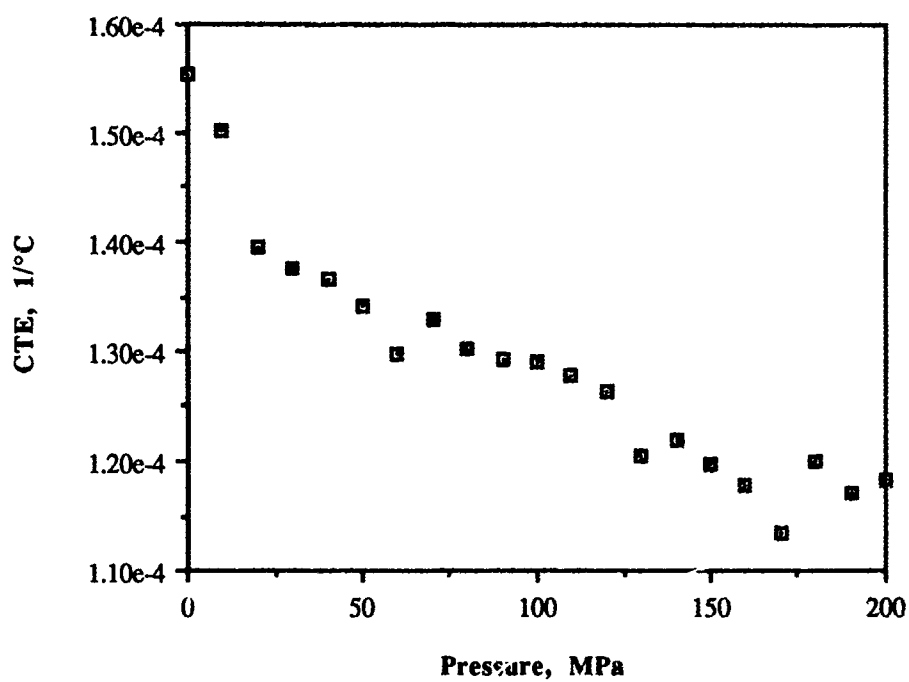


Figure 28. Pressure dependence of the PBO/PEEK CTE.

pressures, there is an axis shift for HTA (amorphous polymer), and there is no increase in pressure and T_g until higher pressures for the semicrystalline polymers tested.

CHAPTER 5

PITCH RESULTS

a. A-240

The 10 MPa isobaric specific volume curve for Ashland's A-240 Pitch is shown in Figure 29. The A-240 system behaves as if it is a material undergoing a melting process. The volumetric transition begins at approximately 65°C and continues through 80°C. In conventional polymer phenomenology, one would describe this as a melting transition with $T_m = 80^\circ\text{C}$. Ashland in fact reports A-240 to have a T_g of 80°C and a softening point of 119°C, but no melt temperature. To further investigate this transition, DSC was performed on the A-240 specimen at 3°C/min. This heating rate is the same as that used by the dilatometer, thus emulating the isobaric volumetric dilatometry scan. The DSC data for the A-240 system, shown in Figure 30, indicate that the transition is endothermic, as we would expect for a melting process, and peaks at 69°C, agreeing with the transition indicated by the $V(T)$ data.

b. A-60

The data from the 10 MPa isobaric scan of Ashland's A-60 Pitch are displayed in Figure 31. The A-60 system is very similar to the A-240, with the exception that the apparent melting transition occurs at a higher temperature. There is a volumetric transition beginning at 88°C and continuing through 97°C. The DSC data for A-60, shown in Figure 32, clearly indicate an endothermic transition centered at 90°C.

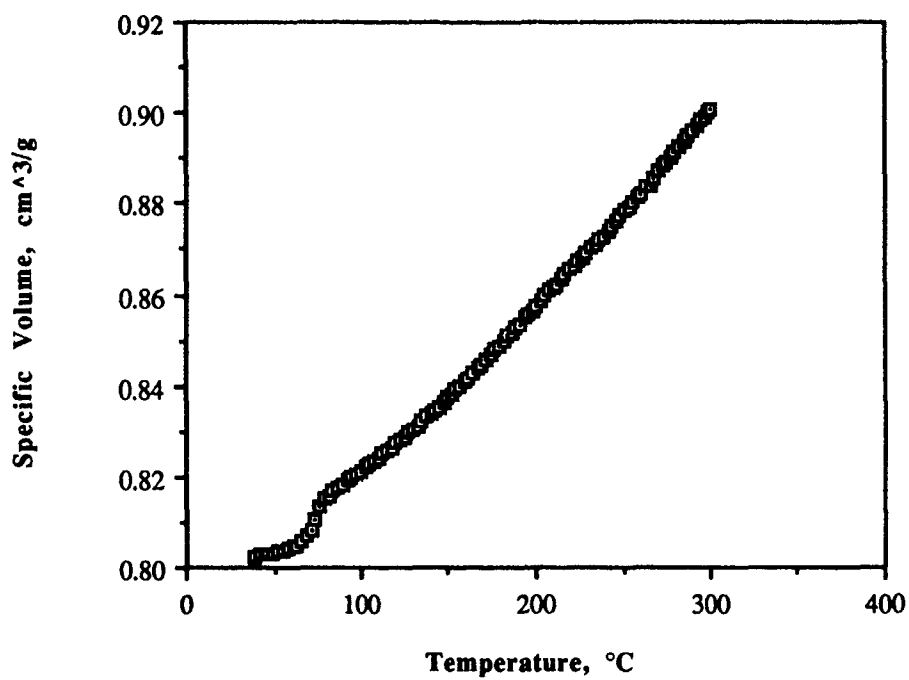


Figure 29. 10 MPa isobaric scan of Ashland's A-240 Pitch.

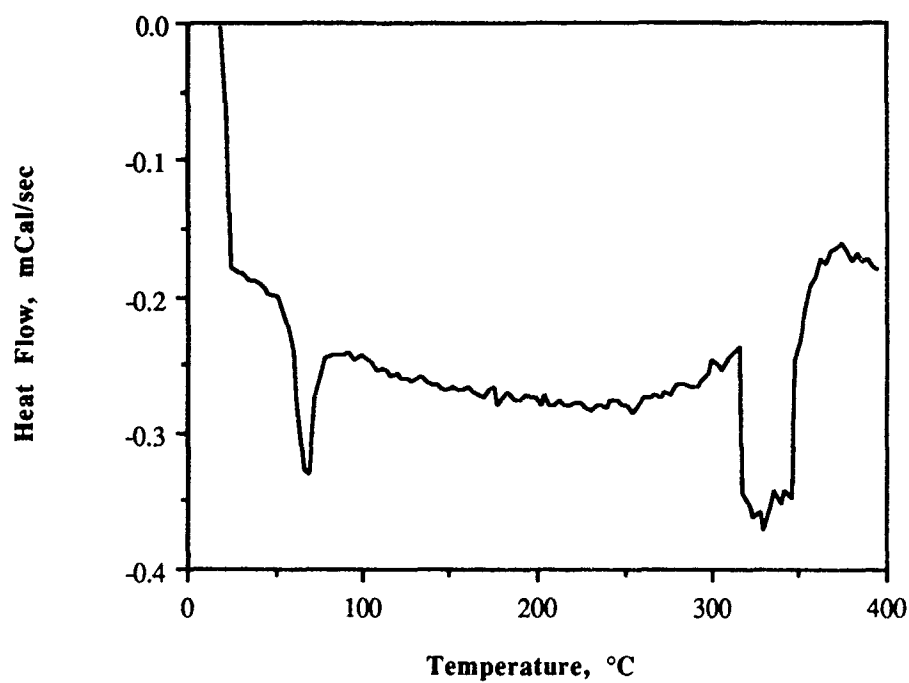


Figure 30. DSC scan of Ashland's A-240 Pitch.

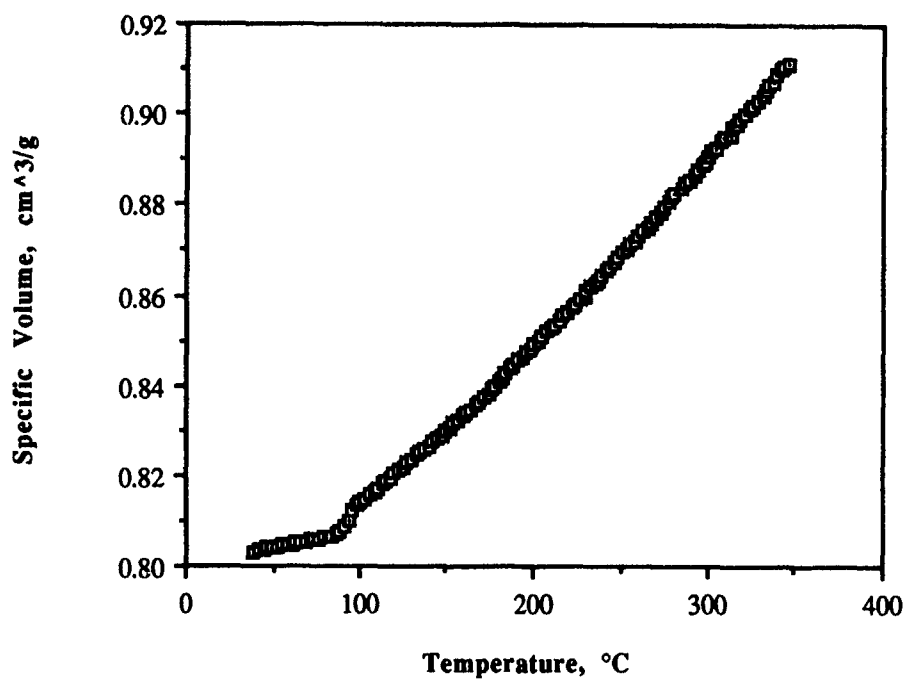


Figure 31. Ten MPa isobaric scan of Ashland's A-60 Pitch.

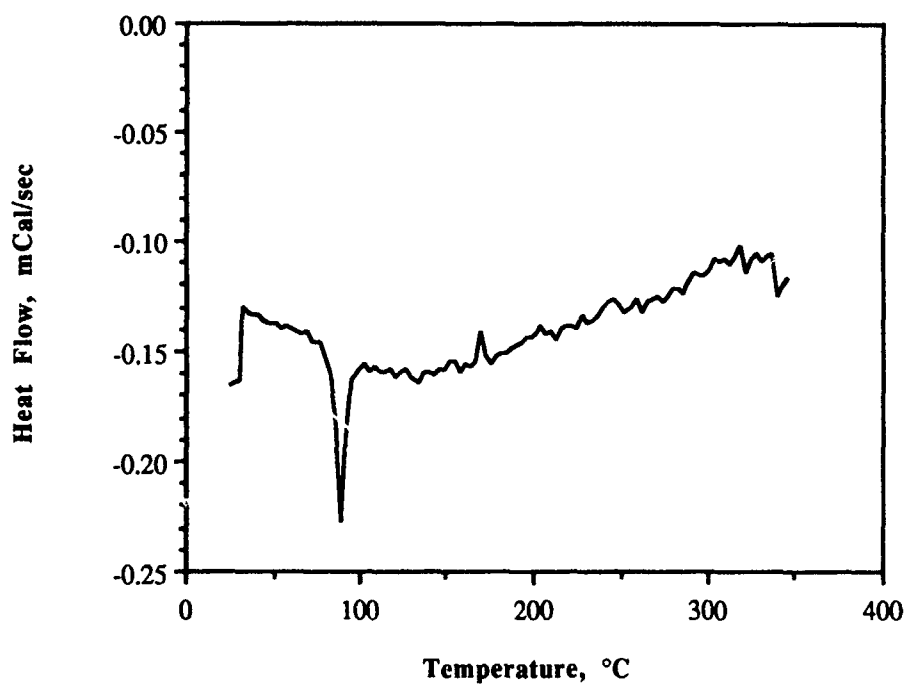


Figure 32. DSC scan of Ashland's A-60 Pitch.

c. A-70

The 10 MPa isobaric scan of Ashland's A-70 Pitch is displayed in Figure 33. Unlike the A-240 or the A-60, the A-70 system exhibits no melting-like transition, but rather has a transition in the $\partial V/\partial T|_{P_0}$ curve at 140°C very much like an amorphous polymer glass transition indicating the change in coefficient of thermal expansion between the glassy and rubbery states of the polymer. The DSC scan (Figure 34) does not indicate any endothermic transitions as seen in A-240 and A-60, but a polymer "T_g-like" baseline shift beginning at 140°C.

d. A-80

The 10 MPa isobaric scan of Ashland's A-80 Pitch is displayed in Figure 35. The A-80 system demonstrated a volumetric transition with low temperature and high temperature linear (relatively) thermal expansion regions. Tangent lines to the low and high temperature regions intersect at 223°C. Ashland Oil, Inc. reports the T_g of A-80 as 224°C. the DSC scan of A-80 is displayed in Figure 36. As with A-70, the A-80 DSC scan has a polymer "T_g-like" baseline shift present from 180 to 200°C.

e. Reilly Coal Tar

The 10 MPa isobaric scan of Reilly Coal Tar Pitch is displayed in Figure 37. The Reilly Coal Tar $V(T)_{P_0}$ curve does not indicate any phase transitions that manifest themselves as specific volume changes. This is also reflected in the DSC scan (Figure 38).

f. Mitsubishi AR Synthetic Mesophase

The 10 MPa isobaric scan of Mitsubishi's AR Synthetic Mesophase Pitch is displayed in Figure 39. The $V(T)_{P_0}$ curve indicates a polymer like glass transition around 175°C. This phenomenon is confirmed by DSC (Figure 40) which shows a baseline shift also beginning around 175°C.

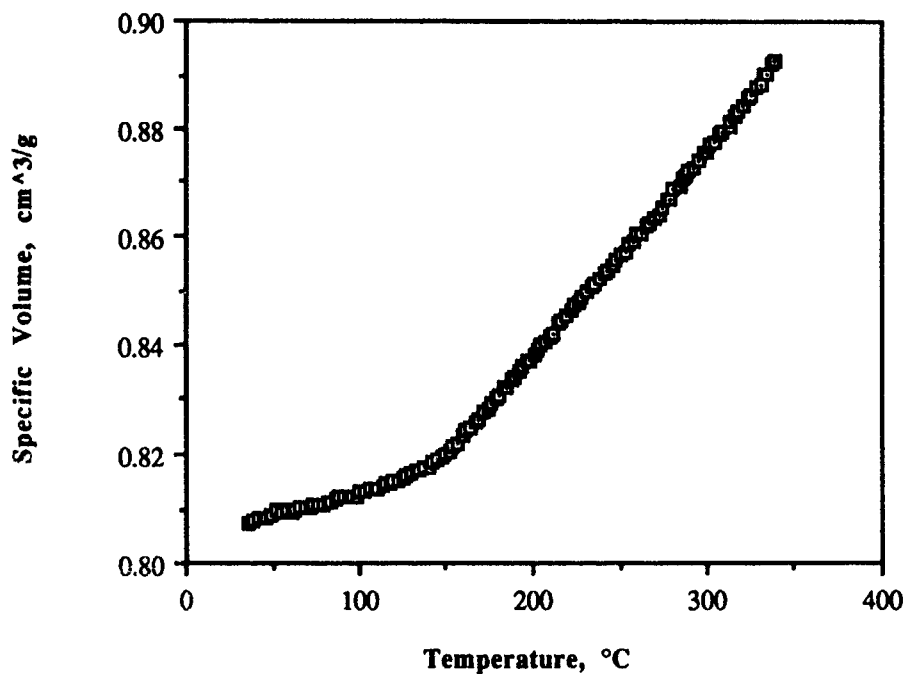


Figure 33. Ten MPa isobaric scan of Ashland's A-70 Pitch.

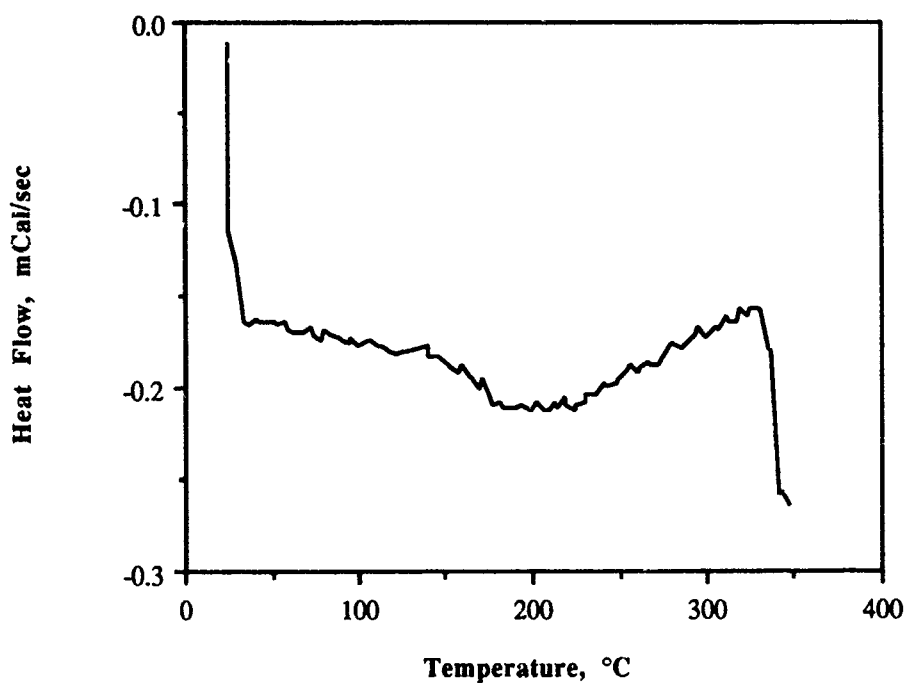


Figure 34. DSC scan of Ashland's A-70 Pitch.

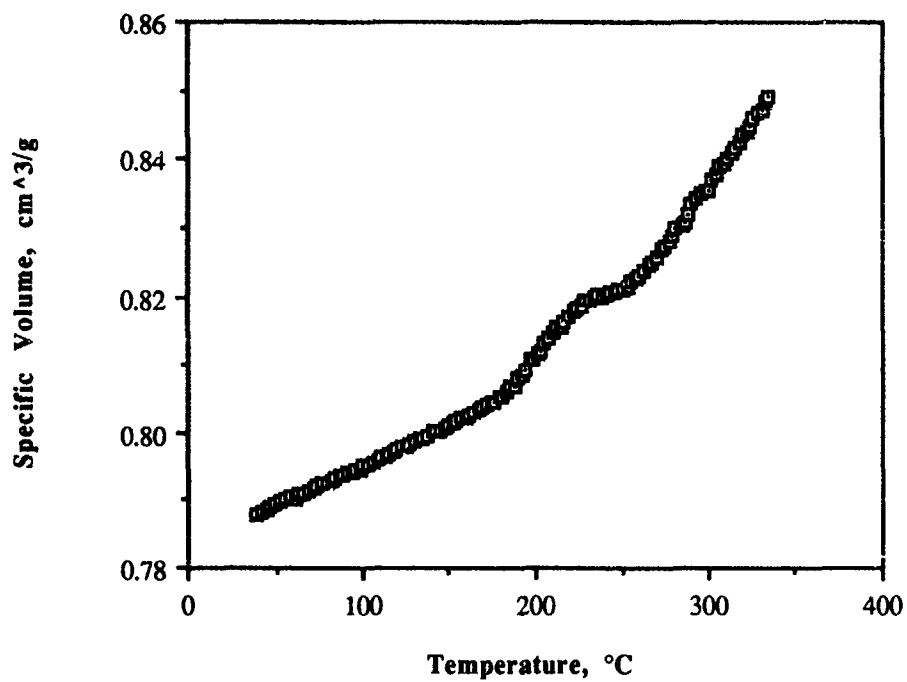


Figure 35. Ten MPa isobaric scan of Ashland's A-80 Pitch.

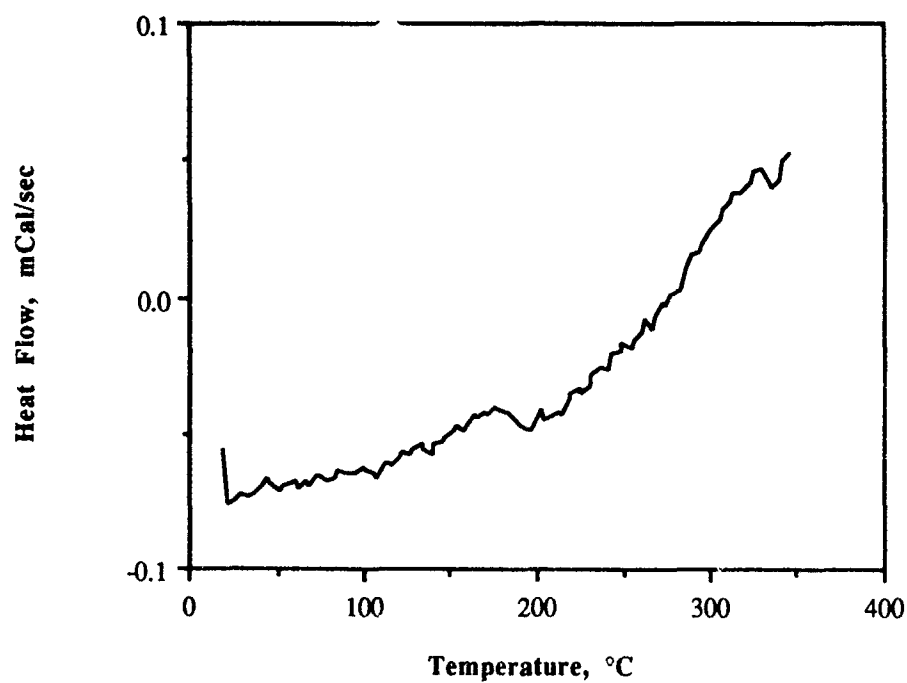


Figure 36. DSC scan of Ashland's A-80 Pitch.

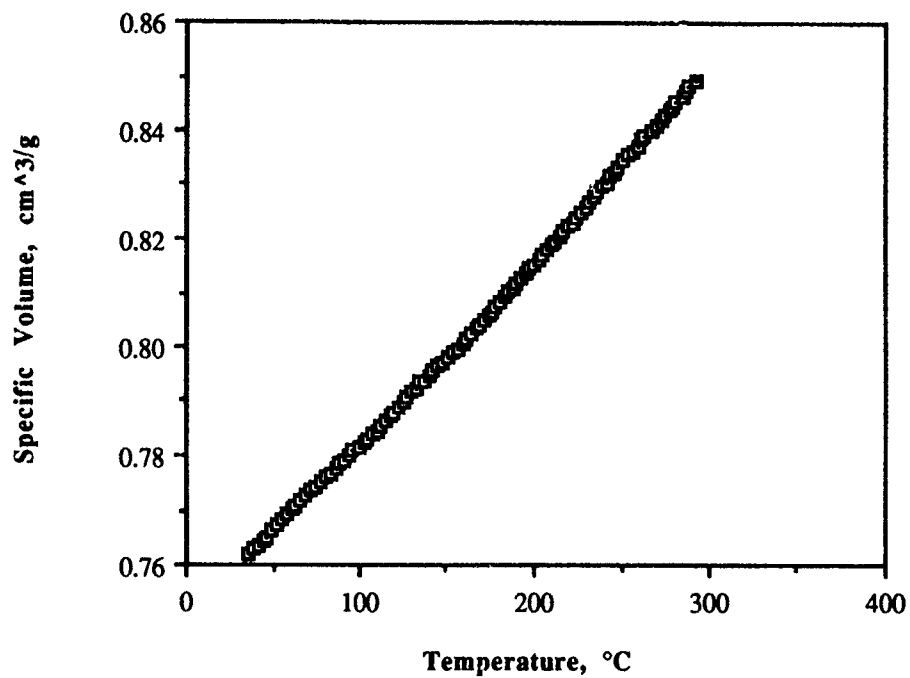


Figure 37. Ten MPa isobaric scan of Reilly Coal Tar Pitch.

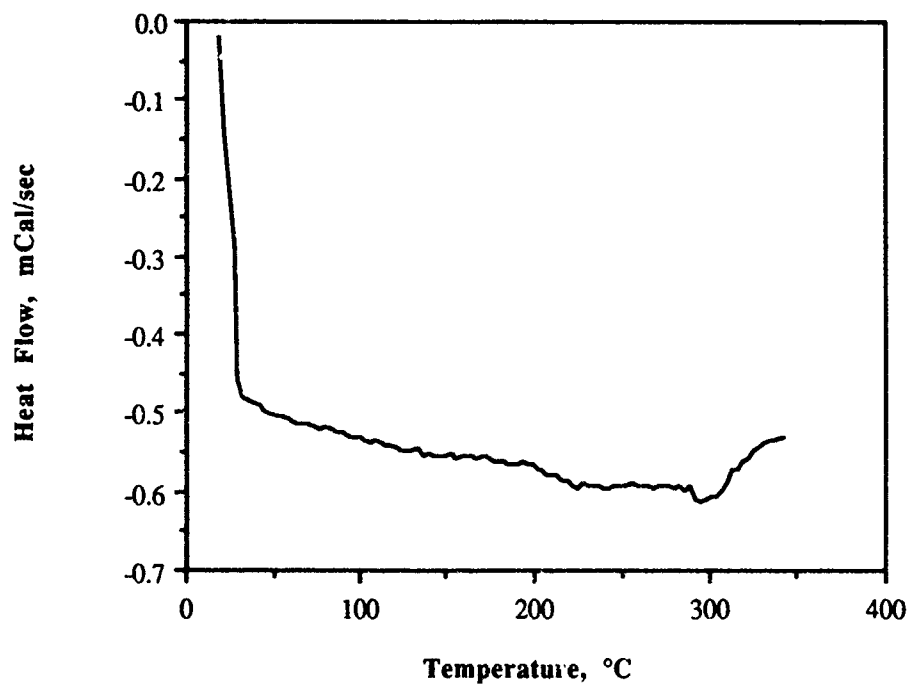


Figure 38. DSC scan of Reilly Coal Tar Pitch.

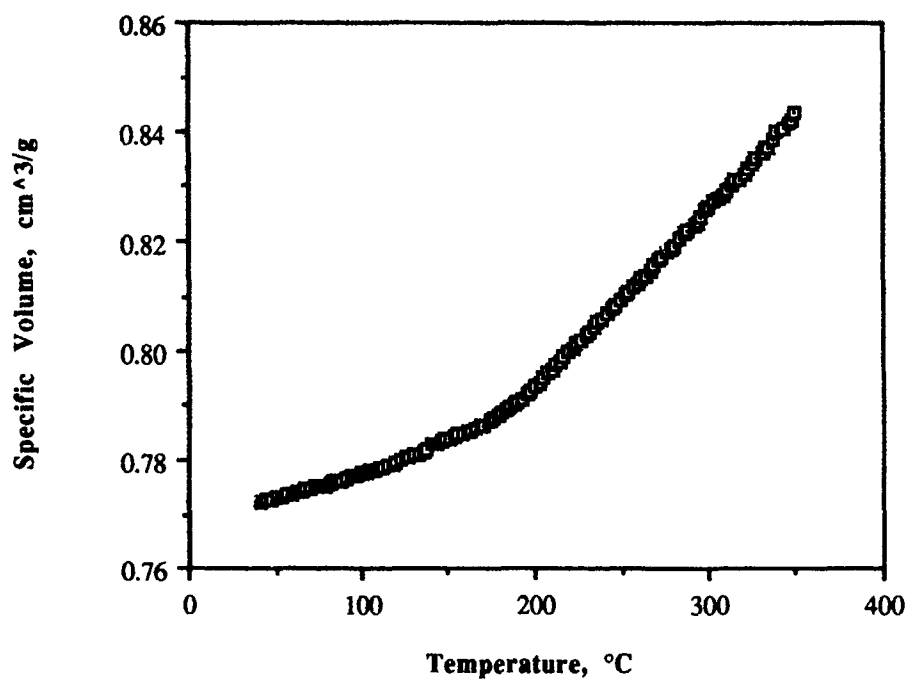


Figure 39. Ten MPa isobaric scan of Mitsubishi's AR Synthetic Mesophase Pitch.

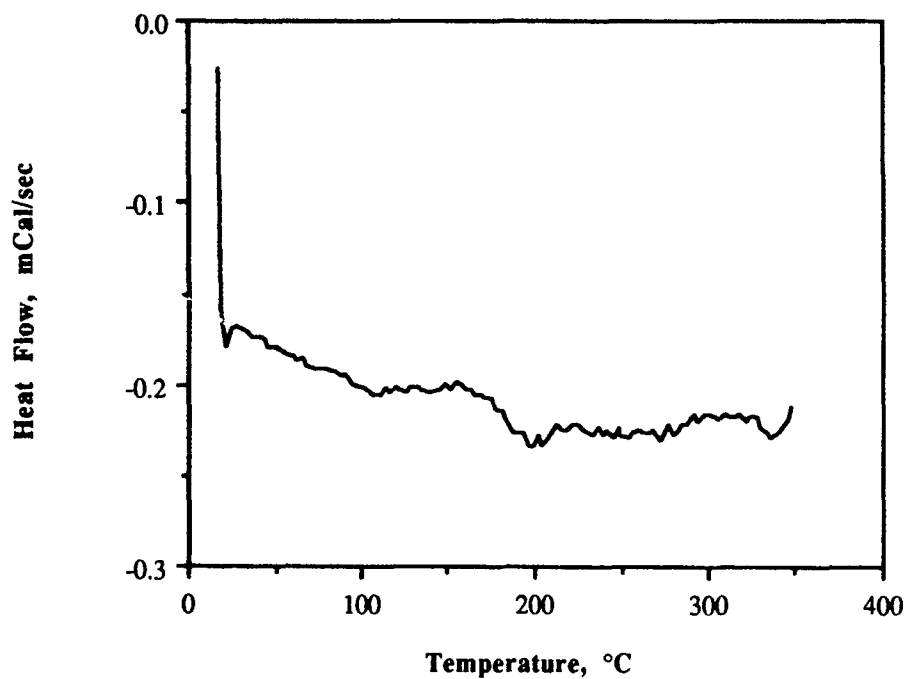


Figure 40. DSC scan of Mitsubishi's AR Synthetic Mesophase Pitch.

g. Conclusions

The types of transitions in the dilatometric data and the temperatures at which they occur have been confirmed by DSC. Both glass transitions, characterized by a change in slope of the $V(T)_{P_0}$ curve, and melting transitions, characterized by a baseline like shift along with a change in slope, were seen in the PVT data of the series of pitches. In general, the thermal expansion of the pitch materials is strongly nonlinear, increasing with increasing temperature. Further analysis is required to confirm the physical origin of the various types of transitions exhibited. They could represent true melting processes or some other type of phase transition.

CHAPTER 6

THERMOSET RESULTS

a. 3501-6

(1) Dilatometry

The specific volumes during a cure cycle of a sample of 3501-6 resin, a sample of AS4/3501-6 prepreg not debulked, and a sample of AS4/3501-6 prepreg vacuum debulked overnight are displayed in Figures 41, 42, and 43 respectively. As expected, the volume change of the prepreg (Figures 42 and 43) was less than the volume change of the resin (Figure 41) due to the presence of the fibers in the prepreg. Both the resin sample and the debulked prepreg sample showed similar responses. First, the specific volume increased due to thermal expansion upon the initial heatup to 116°C (240°F), from 0.8716 to 0.9017 cm³/g for the resin and from 0.6867 to 0.6989 cm³/g for the debulked prepreg. During the 116°C hold, the specific volume decreased due to polymerization, from 0.9017 to 0.8937 cm³/g for the resin and from 0.6989 to 0.6965 cm³/g for the debulked prepreg. Thermal expansion again occurred during the ramp from 116°C to 177°C (350°F). The specific volume increased from 0.8937 to 0.9126 cm³/g for the resin and from 0.6965 to 0.7037 cm³/g for the debulked prepreg. During the 177°C hold, polymerization again caused the specific volume to decrease until near the 200-minute point in the cure cycle, from 0.9126 to 0.8899 cm³/g for the resin and from 0.7037 to 0.6925 cm³/g for the debulked prepreg. At this point, no further shrinkage occurred until the sample was cooled back to room temperature (RT). Had the volume change data been taken during the cooldown below 100°C (212°F), the final volume would have been smaller than the initial volume. At 100°C, the resin specific volumes during initial heatup and during cooldown were

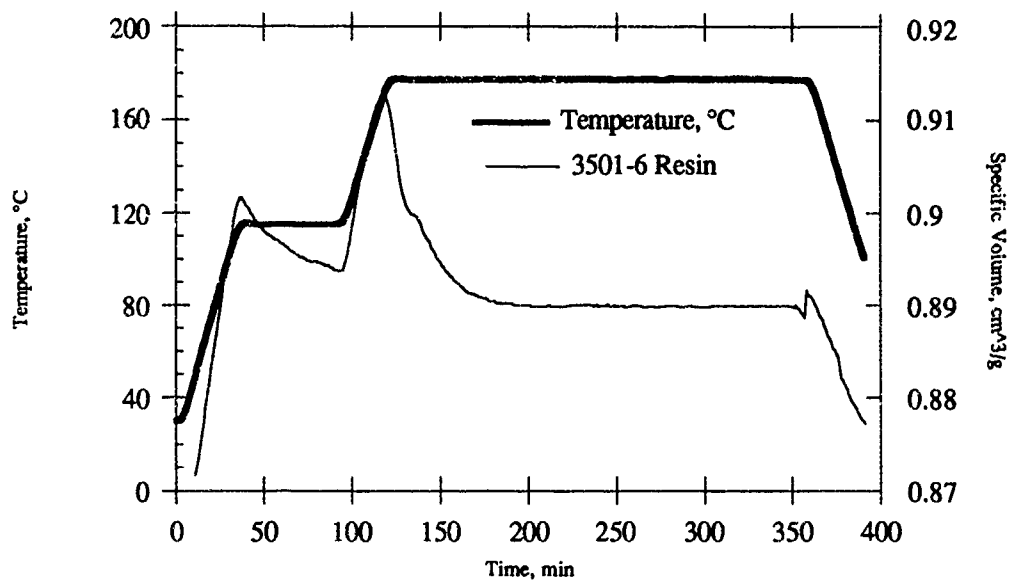


Figure 41. Effect of cure cycle on the volume changes in 3501-6 resin.

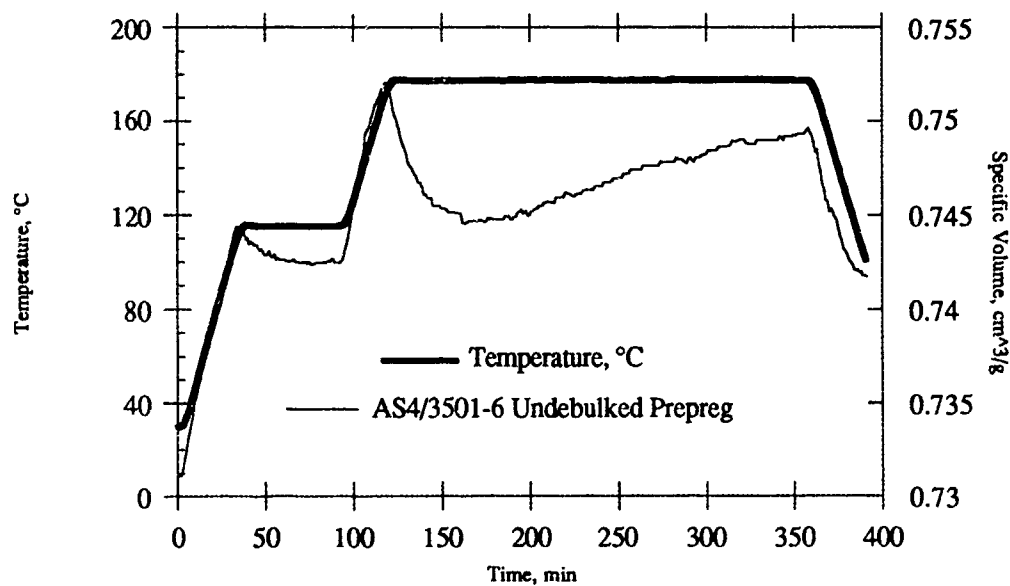


Figure 42. Effect of cure cycle on the volume changes in undebulked AS4/3501-6 prepreg.

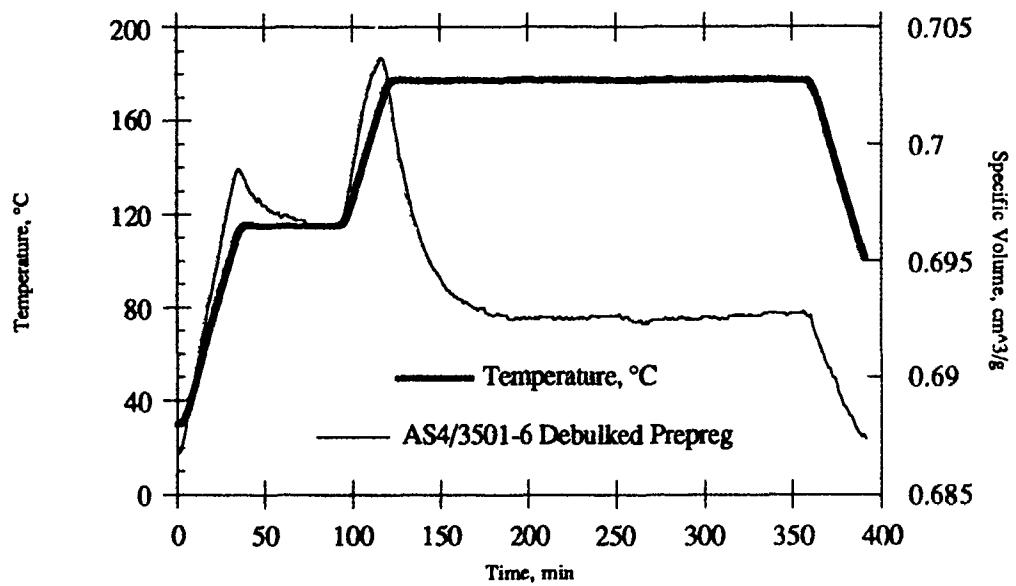


Figure 43. Effect of cure cycle on the volume changes in debulked AS4/3501-6 prepreg.

0.8772 and 0.8951 cm³/g respectively while the debulked prepreg specific volumes during initial heatup and during cooldown were 0.6976 and 0.6874 cm³/g respectively. The sharp decrease then increased in specific volume of the resin near the 350 minute point in the cure cycle as seen in Figure 41 was due to a fluctuation in the pressure applied to the sample. The pressure was returned to 10 MPa by the start of the cooling ramp.

The response of the undebulked sample (Figure 42) was similar to the other two samples until the 177°C hold. First, the specific volume increased due to thermal expansion upon the initial heatup to 116°C from 0.7309 to 0.7444 cm³/g. During the 116°C hold, the specific volume decreased due to polymerization from 0.7444 to 0.7425 cm³/g. Thermal expansion again occurred during the ramp from 116°C to 177°C. The specific volume increased from 0.7425 to 0.7520 cm³/g. During the 177°C hold, the specific volume decreased due to polymerization from 0.7520 to 0.7455 cm³/g at the 160 minute mark. However, the specific volume then increased from 0.7455 to 0.7496 cm³/g until the end of the 177°C hold. As the sample was cooled, the specific volume decreased from 0.7496 cm³/g at 177°C to 0.7417 cm³/g at 100°C. Again, had the volume change data been taken during the cooldown below 100°C, the final volume would have been smaller than the initial volume. At 100°C, the specific volume during initial heatup was 0.7431 cm³/g.

A photomicrograph (PMG) of the cross section of the undebulked sample (Figure 44) displayed gross porosity. The PMG evidence and the dilatometer evidence showing an increase in specific volume after the initial cure shrinkage indicated that void formation and growth was occurring, possibly due to excess moisture absorbed into the prepreg. The vapor pressure of saturated steam at 177°C is approximately 9.35 MPa. Local temperature variations in the sample of only 3°C would have raised the vapor pressure above 10 MPa, the dilatometer's operating pressure. Thus, the large amount of residual moisture in the sample caused the increase in volume during the 177°C hold. Normally during an



Figure 44. PMG of the undebulked AS4/3501-6 prepreg sample cured in the PVT apparatus.

autoclave cure, a vacuum is applied at the beginning of the cure so the excess moisture escapes before the resin polymerizes around the void, creating a hole in the resin.

(2) Rheology

The response of storage modulus (G') and loss modulus (G'') during cure is displayed in Figure 45. The data from the DMA can be correlated to the dilatometric data. G' decreased during the initial ramp to 116°C, and the minimum in G' occurred near the same time into the cure cycle as the maximum in volume change. G' increased slightly during the 116°C hold due to the increased stiffness upon polymerization, thus confirming the dilatometric data. G' decreased again during the ramp from 116 to 177°C, and another minimum in G' occurred near the same time into the cure cycle as the maximum in volume change. During the 177°C hold, G' first increased rapidly and then leveled off near the 200-minute point in the cure cycle. This again confirmed the dilatometric data showing polymerization during the 177°C hold. One difference between the dilatometric data and the DMA data was that while the resin and debulked prepreg showed little or no further shrinkage after 200 minutes into the cure cycle, the DMA data showed a gradual increase in G' during this period. This would indicate further crosslinking was occurring to cause the gradual increase in the storage modulus.

(3) Microdielectrometry

The response of the dielectric loss factor ($E2$) at several frequencies during an autoclave cure of AS4/3501-6 prepreg is displayed in Figure 46. The $E2$ data can also be correlated to the dilatometric data. $E2$ increased during the initial ramp to 116°C, and the maximum in $E2$ occurred near the same time as the maximum in volume change. $E2$ decreased during the 116°C hold indicating reduced mobility from the onset of polymerization. This can be correlated to the reduction in volume during the 116°C hold from polymerization shrinkage. $E2$ then increased during the ramp from 116 to 177°C, and another maximum in $E2$ occurred at the same time into the cure cycle as the maximum in

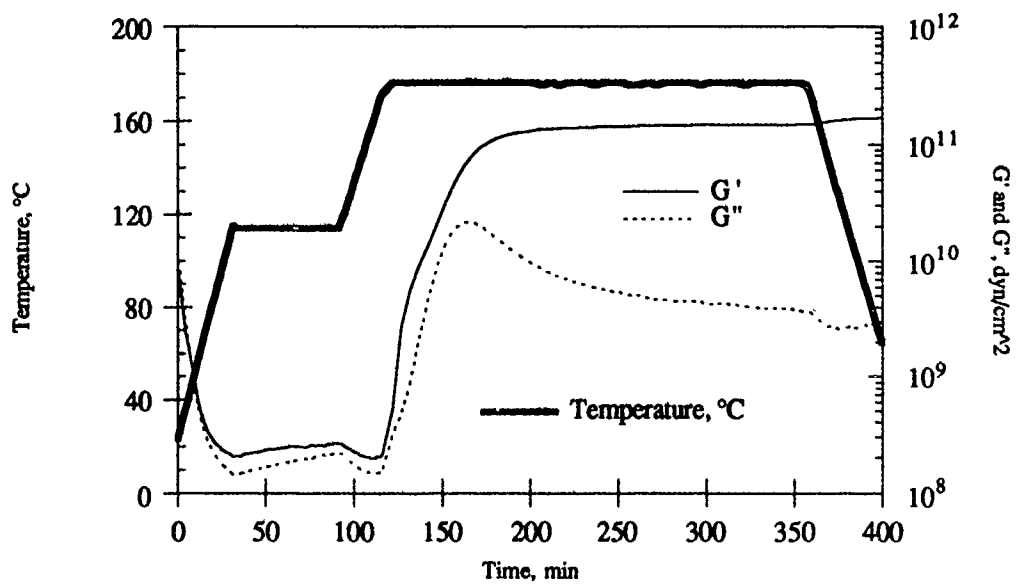


Figure 45. DMA scan of AS4/3501-6 prepreg.

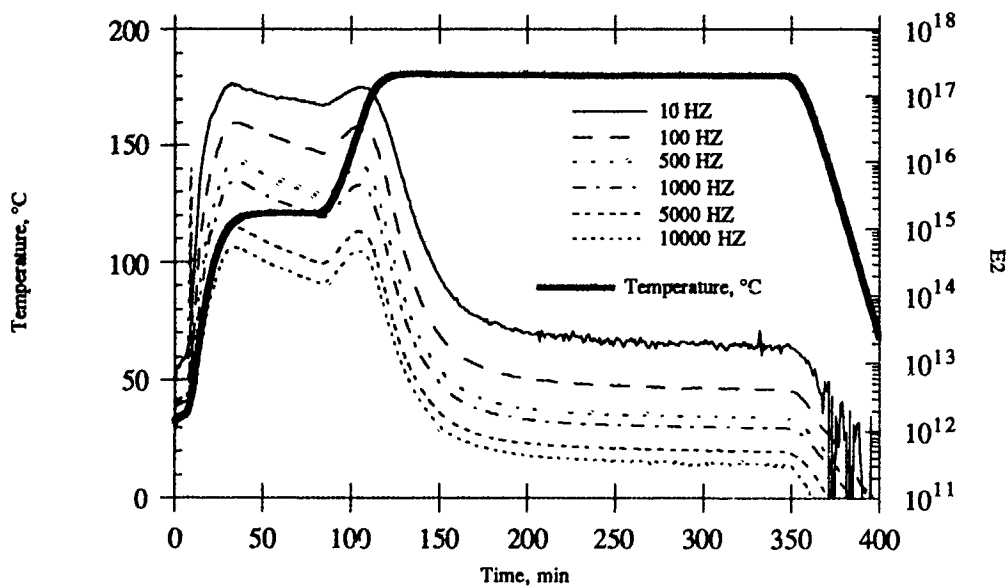


Figure 46. Dielectric loss factor response of AS4/3501-6 prepreg during cure.

volume change. During the 177°C hold, E2 decreased rapidly and then leveled out near the 200-minute point in the cure cycle. This confirmed the dilatometric data showing the polymerization during the 177°C hold. After the 200-minute point in the cure cycle, E2 continued to gradually decrease because of decreased ion mobility due to crosslinking while there was little or no further volume shrinkage. These data, in conjunction with the increase in G' during the same period, indicated that further crosslinking is taking place. However, the constant specific volume in that period indicated that the bulk of the polymerization had been completed. The bulk of the crosslinking would be between adjacent polymer chains and would not use any free monomers.

b. 8551-7A

(1) Dilatometry

The volume change during the cure of IM7/8551-7A prepreg is displayed in Figure 47. The sample was vacuum debulked overnight. The response of the volume change of the prepreg to the cure cycle was similar to the AS4/3501-6 response. This would be expected because both are epoxies. First, the specific volume increased due to thermal expansion upon the initial heatup to 116°C from 0.7433 to 0.7572 cm³/g. During the 116°C hold, the specific volume decreased due to polymerization from 0.7572 to 0.7551 cm³/g. Thermal expansion again occurred during the ramp from 116°C to 177°C. The specific volume increased from 0.7551 to 0.7644 cm³/g. During the 177°C hold, the specific volume initially decreased due to polymerization from 0.7644 to 0.7503 cm³/g at the 160 minute mark. The specific volume then increased slightly from 0.7503 to 0.7514 cm³/g at the 250-minute point in the cure. The specific volume then was constant throughout the remainder of the 177°C hold. This may have been due to residual moisture still left in the prepreg. As the sample was cooled, the specific volume decreased from 0.7514 cm³/g at 177°C to 0.7441 cm³/g at 100°C. Again, had the volume change data been

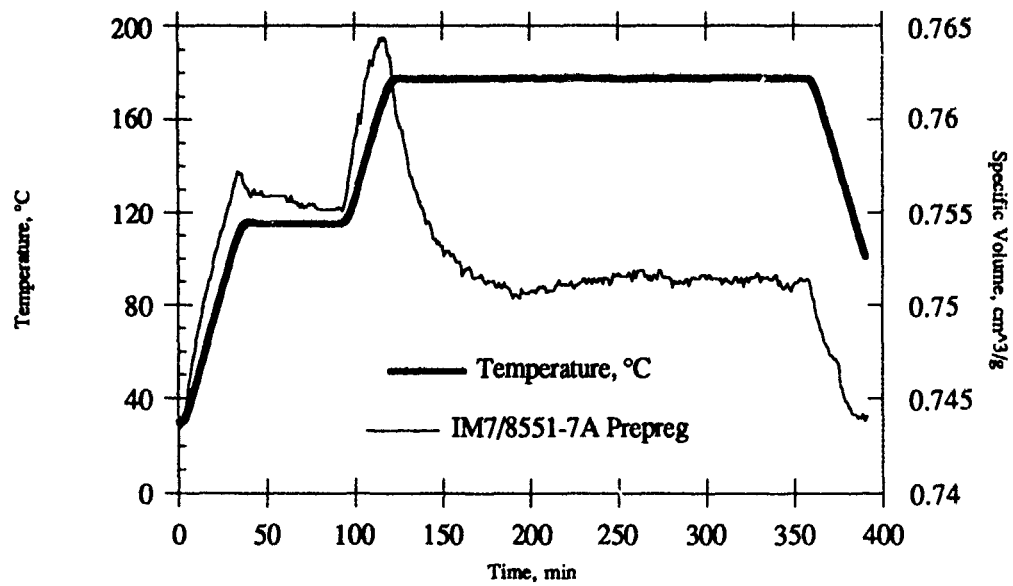


Figure 47. Effect of cure cycle on the volume changes in IM7/8551-7A prepreg.

taken during the cooldown below 100°C, the final volume would have been smaller than the initial volume. At 100°C, the specific volume during initial heatup was 0.7557 cm³/g.

(2) Rheology

The response of storage modulus (G') and loss modulus (G'') during cure is displayed in Figure 48. The minimums in G' and the rapid increase in G' during the 177°C hold corresponded to events in the dilatometric data. G' did increase slightly after the 200 minute point in the cure cycle, while the volume became constant in the same region. This would again indicate that further crosslinking was occurring, thereby increasing G', while not using any free monomers and causing the matrix to shrink.

(3) Microdielectrometry

The response of the dielectric loss factor of IM7/8551-7A during the cure is displayed in Figure 49. The maximums in E2 and the rapid decrease of E2 during the 177°C hold corresponded to events in the dilatometric data. However, after the 200-minute point in the cure cycle, E2 actually increased gradually at the lower frequencies while E2 decreased at the higher frequencies. Despite the gradual increase of E2 at the lower frequencies, both the DMA data and the high frequency E2 data indicated further crosslinking is occurring, just as with 3501-6.

c. 5250-4

(1) Dilatometry

The volume change during the cure of IM7/5250-4 prepreg is displayed in Figure 50. The sample was vacuum debulked overnight. There was some differences between the behavior of the BMI and the epoxies. First, the specific volume increased due to the DSC scan (Figure 51). Thermal expansion again occurred during the ramp from 116°C to 177°C. The specific volume increased from 0.7728 to 0.7849 cm³/g. The resin did not finish shrinking during the 177°C hold. This indicated slower polymerization

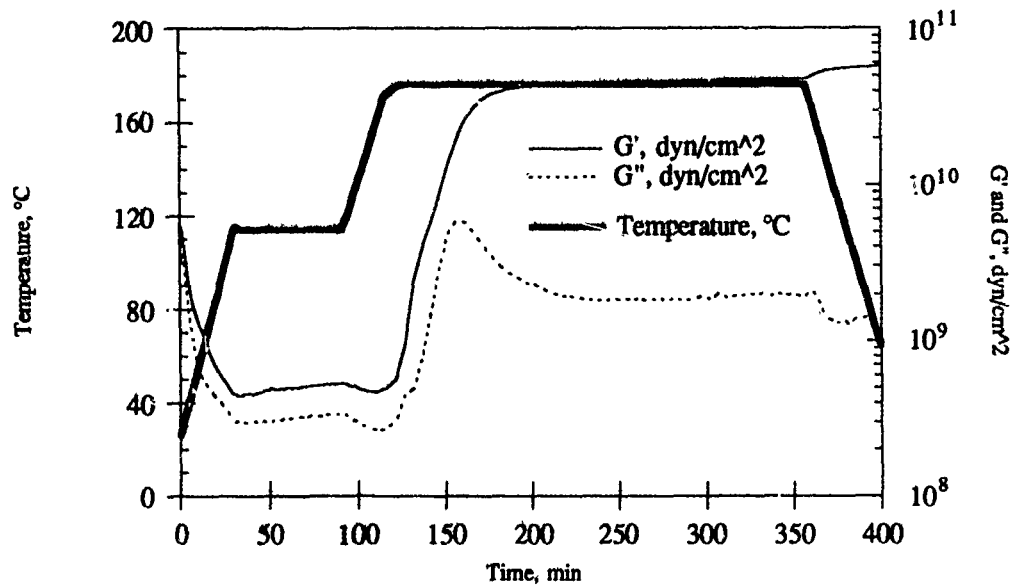


Figure 48. DMA scan of IM7/8551-7A prepreg.

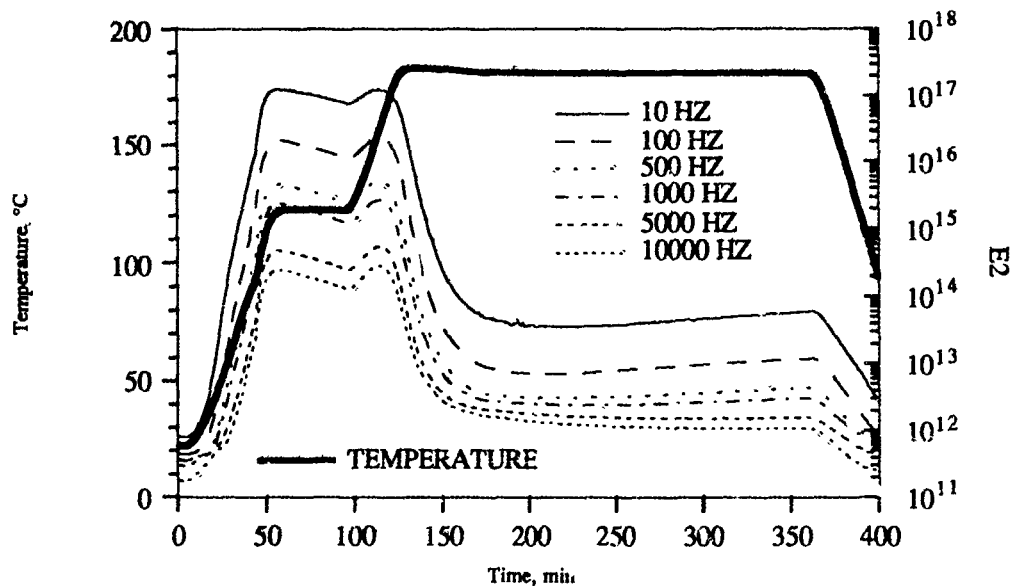


Figure 49. Dielectric loss factor response of IM7/8551-7A prepreg during cure.

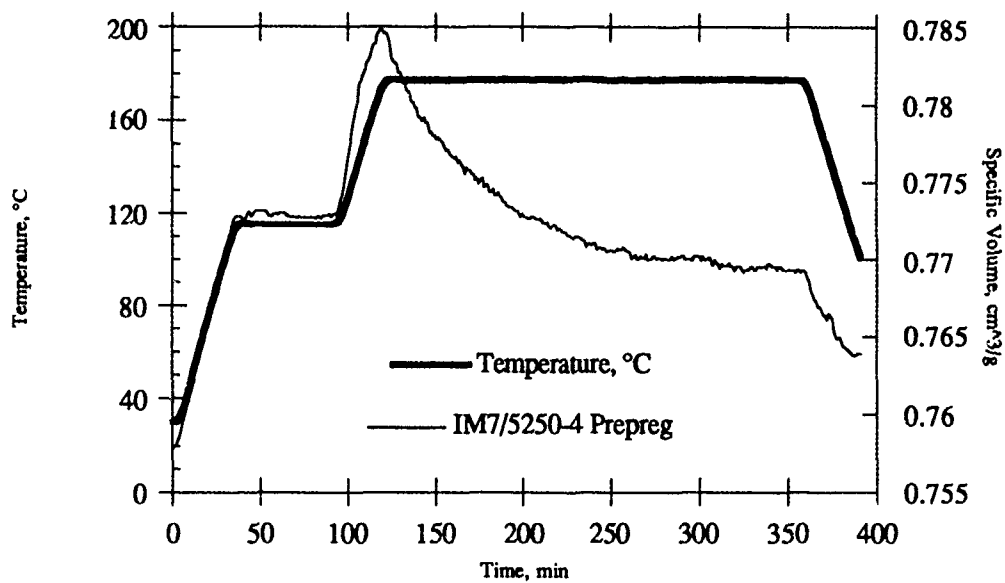


Figure 50. Effect of cure cycle on the volume changes in IM7/5250-4 prepreg.

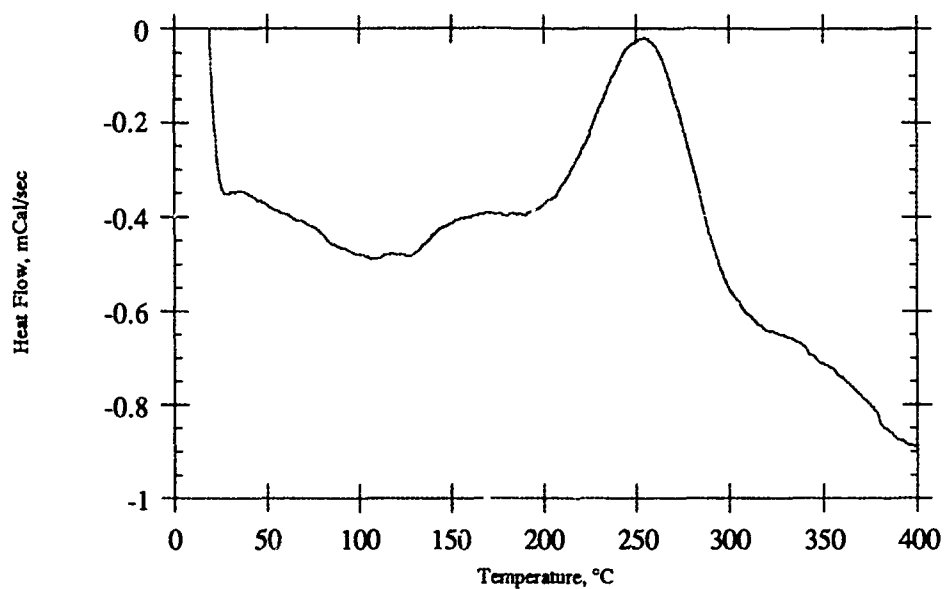


Figure 51. DSC scan of IM7/5250-4 prepreg.

kinetics than the epoxies. This would also be expected because the DSC scan indicated the bulk of the reaction did not begin to occur until near 200°C (396°F) and the reaction peak occurred near 255°C (490°F). The 5250-4 must be oven postcured at 227°C (440°F) for 6 hours to fully crosslink the matrix. At the end of the hold, the specific volume was 0.7693 cm³/g. As the sample was cooled, the specific volume decreased from 0.7693 cm³/g at 177°C to 0.7639 cm³/g at 100°C. Again, had the volume change data been taken during the cooldown below 100°C, the final volume would have been smaller than the initial volume. At 100°C, the specific volume during initial heatup was 0.7700 cm³/g.

(2) Rheology

The response of storage modulus (G') and loss modulus (G'') during cure is displayed in Figure 52. The constant G' value during the 116°C hold corresponded with the constant volume found from the dilatometric data. Also, G' increased more slowly than the epoxies did during the 177°C hold and just began to level off at the end of the hold. This confirmed the slow matrix shrinkage seen with the dilatometric data indicating slow polymerization kinetics.

(3) Microdielectrometry

IM7/5250-4 was not autoclave cured in this study. However, work at McDonnell Douglas³⁵ using dielectric cure monitoring of 5250-4 prepreg using a similar cure cycle to this study confirmed the dilatometric data and the rheological data. No dielectric response was seen in the 116°C hold, while the dielectric response was slow to level off during the 177°C hold due to the slow polymerization kinetics.

d. Conclusions

The cure shrinkage of thermoset resin prepreps was studied with a volumetric dilatometer. Volumetric dilatometry can be a useful tool in studying resin characteristics during cure for several reasons. First, distinct regions of thermal expansion and

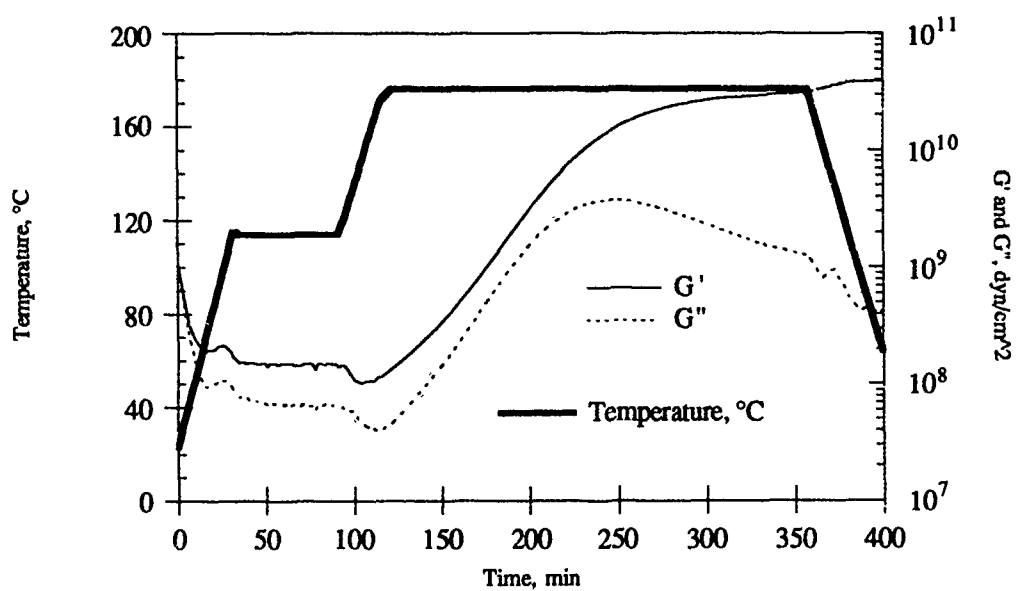


Figure 52. DMA scan of IM7/5250-4 prepreg.

polymerization shrinkage were seen. These data can be used to study residual stress buildup during cooldown from cure. These data also compared well with events from DMA scans and from dielectric measurements during autoclave curing. Furthermore, void formation and growth was seen in a composite sample which was not vacuum debulked to remove residual water absorbed by the resin. Finally, the sample size is smaller than a sample for DMA. Drawbacks are that further crosslinking after the bulk of the monomers were polymerized cannot be seen with dilatometry. Therefore, degree of cure cannot be accurately determined. Another drawback is that mercury, which is used as a confining fluid in the dilatometer, is a toxic material and must be handled and disposed of with care.

CHAPTER 7

CONCLUSIONS

A volumetric dilatometer was used to measure the PVT properties of thermoplastic polymers, pitch based precursors for carbon-carbon composites, and thermoset polymers and their composites. For the thermoplastic polymers, T_g , T_m , and T_c were identified and were found to increase with increasing pressure. The coefficient of thermal expansion (CTE) as a function of pressure of both polymers was found in the glassy regions. The formation of densified glasses was seen when polymers in the melt state were compressed. For the pitches, T_g and T_m were identified using the PVT apparatus and confirmed by DSC. For the thermoset polymers and composites, distinct regions of cure shrinkage and thermal expansion were seen. These data were confirmed by DMA and dielectric cure monitoring.

a. Future Work

(1) Morphology of Densified PEEK

After isobaric cooling of PEEK under high pressure, the polymer was much denser than the original polymer formed at low pressures. The high pressure may affect the crystalline morphology which in a composite could affect the mechanical properties. The effect of pressure on the crystalline morphology of PEEK should be studied.

(2) Dilatometric Study of APC-2 Under Different Processing Conditions

Previous work has been done in characterizing the properties of APC-2 composites (AS4/PEEK) under different processing conditions, including slow cooling and

quenching^{26,37}. Changing the processing conditions from slow cooling to quenching will change the morphology of the polymer from semicrystalline to amorphous. The mechanical and physical properties will change with the change in morphology. The PVT properties of APC-2 processed under different conditions should be studied.

(3) Dilatometric Study of Condensation Curing Resins

Condensation curing resins give off byproducts during the polymerization. These types of resins provide an added complexity to processing. The volume change during the cure and postcure of AFR700, a fluorinated polyimide, will be studied. Difficulties could occur due to the volume changes of the reaction byproducts, water and methanol, masking the volume changes of the polymer.

REFERENCES

1. Ferry, J.D. Viscoelastic Properties of Polymers. 3rd ed. New York: Wiley and Sons, 1980.
2. Kovacs, A.J. "La contraction isotherme du volume des polymers amorphes." J. Polym. Sci. 30 (1958): 131-147.
3. Struik, L.C.E. Physical Aging in Amorphous Polymers and Other Materials. Amsterdam: Elsevier, 1978.
4. Bueche, F. "Bulk Viscosity of the System Polystyrene-Diethyl Benzene." J. Appl. Phy. 24, no. 4 (1953): 423-427.
5. Fox, T.G., and P.J. Flory. "Second-Order Transition Temperatures and Related Properties of Polystyrene. I. Influence of Molecular Weight." J. Appl. Phy. 20 (June 1950): 581-591.
6. McLoughlin, J., and A.V. Tobolsky. "Effect of Rate of Cooling on Stress Relaxation of Polymethyl Methacrylate." J. Polym. Sci. 7 (1951): 658.
7. Nairn, J.A., and P. Zoller. "The Development of Residual Thermal Stresses in Amorphous and Semicrystalline Thermoplastic Matrix Composites." Edited by N.J. Johnston. Toughened Composites. ASTM STP 937. Philadelphia: ASTM, 1987.
8. Blundell, D.J., and B.N. Osborn. "Crystalline Morphology of the Matrix of PEEK-Carbon Fiber Aromatic Polymer Composites. II..Crystallization Behavior." SAMPE Quarterly 17, no. 1 (1985): 1-6.
9. Zoller, P. "Specific Volume of Polysulfone as a Function of Temperature and Pressure." J. Polym. Sci. Polym. Phys. Ed. 16 (1978): 1261-1275.

10. Zoller, P., P. Bolli, V. Pahud, and H. Ackermann. "Apparatus for Measuring Pressure-Volume-Temperature Relationships of Polymers to 350°C and 220 kg/cm²." Rev. Sci. Instrum. 47, no. 8 (1976): 948-952.
11. Quach, A., and R. Simha. "Pressure-Volume-Temperature Properties and Transitions of Amorphous Polymers; Polystyrene and Poly(orthomethylstyrene)." J. Appl. Phys. 42, no. 12 (1971): 4592-4606.
12. McKinney, J.E., and M. Goldstein. "PVT Relationships for Liquid and Glassy Poly(vinyl acetate)." J. Res. Nat. Bur. Stand. 78A (1974): 331-353.
13. McKinney, J.E., and R. Simha. "Configurational Thermodynamic Properties of Polymer Liquids and Glasses. I. Poly(vinyl acetate)." Macromol. 7 (1974): 894-901.
14. McKinney, J.E., and R. Simha. "Configurational Thermodynamic Properties of Polymer Liquids and Glasses. Poly(vinyl acetate). II." Macromol. 9 (1976): 430-442.
15. Zoller, P., and H.H. Hoehn. "Pressure-Volume-Temperature Properties of Blends of Poly(2,6-dimethyl-1,4-phenylene Ether) with Polystyrene." J. Polym. Sci. Polym. Phys. Ed. 20 (1982): 1385-1397.
16. Zoller, P. "A Study of the Pressure-Volume-Temperature Relationships of Four Related Amorphous Polymers: Polycarbonate, Polyarylate, Phenoxy, and Polysulfone." J. Polym. Sci. Polym. Phys. Ed. 20 (1982): 1453-1464.
17. Zoller, P. "PVT Relationships and Equations of State of Polymers." Edited by J. Brandrup and E.H. Immergut. Polymer Handbook. 3rd ed. New York: Wiley and Sons, 1989.
18. Zoller, P., T.A. Kehl, H.W. Starkweather, Jr., and G.A. Jones. "The Equation of State and Heat of Fusion of Poly(ether ether ketone)." J. Polym. Sci. Polym. Phys. Ed. 27 (1989): 993-1007.

19. Starkweather, H.W. Jr., P. Zoller, G.A. Jones, and A.J. Vega. "The Heat of Fusion of Polytetrafluoroethylene." J. Polym. Sci. Polym. Phys. Ed. 20 (1982): 751-761.
20. Zoller, P. "The Specific Volume of Poly(tetrafluoroethylene) as a Function of Temperature (30°-372°C) and Pressure (0-2000 kg/cm²)." J. Appl. Polym. Sci. 22 (1978): 633-641.
21. Zoller, P. "The Pressure-Volume-Temperature Properties of Three Well-Characterized Low-Density Polyethylenes." J. Appl. Polym. Sci. 23 (1979): 1051-1056.
22. Zoller, P., and P. Bolli. "Pressure-Volume-Temperature Properties of Solid and Molten Poly(ethylene Terephthalate)." J. Macromol. Sci. Phys. B18, no. 3 (1980): 555-568.
23. Curro, J.G. "Polymeric Equations of State." J. Macromol. Sci.-Revs. Macromol. Chem. C11 (1974): 321-366.
24. Kroekel, C.H., and E.L. Bartkus. "Low Shrink Polyester Resins: Performance and Application." Annual Conference, Reinforced Plastics/Composites Institute. Brookfield Center CT: SPI, (1968).
25. Daniel, I.M., T.-M. Wang, D. Karalekas, and J.T. Gotro. "Determination of Chemical Cure Shrinkage in Composite Laminates." J. of Composites Tech. and Res. 12, no. 3 (1990): 172.
26. Rodriquez, F. Principles of Polymer Systems. 3rd ed. New York: Hemisphere, 1989.
27. Bromberg, M.L., D.R. Day, and K.R. Snable. "Measurement and Application of Dielectric Properties." IEEE Electr. Insul. Mag. 2, no. 3 (1986): 18.
28. Bidstrup, W.W., N.F. Sheppard, Jr., and S.D. Senturia. "Monitoring of Laminate Cure with Microdielectrometry." Polymer Engineering and Science. 26, no. 5 (1986): 358.

29. Sanjana, Z.N. "The Use of Microdielectrometry in Monitoring the Cure of Resins and Composites." Polymer Engineering and Science. 26, no. 5 (1986): 373.
30. Day, D.R. "Effects of Stoichiometric Mixing Ratio on Epoxy Cure -- a Dielectric Analysis." Polymer Engineering and Science. 26, no. 5 (1986): 362.
31. Anderson, D.P. "Crystalline Morphology of APC/HTX Materials via X-ray Diffraction." Proceedings of the SPE 47th Annual Technical Conference. 1989.
32. Bridgman, P.W. The Physics of High Pressures. London: Bell, 1952.
33. Russell, J.D. "Analysis of Viscoelastic Properties of High-Temperature Polymers Using a Thermodynamic Equation of State." M.S. Thesis, University of Dayton, 1991.
34. The Dow Chemical Company. Thermoplastic Molecular Composite Development. USAF Contract F33615-86-C-5068.
35. McDonnell Douglas Corporation. Advanced Composite Processing Technology Development. USAF Contract F33615-88-C-5455.
36. Russell, J.D., and D.B. Curliss. "Effects of Different Thermal Histories on the Mechanical Properties and Fracture Toughness of APC-2." 23rd International SAMPE Technical Conference, Kiamesha Lake NY, 22-24 October 1991.
37. Sichina, W., and P.S. Gill. "Characterization of Composites Using Dynamic Mechanical Analysis." 33rd International SAMPE Symposium, Anaheim CA, 7-10 March 1988.